AFOSR-TR-97

0326

REPORT DOCUMENTATION P

1. AGENCY USE ONLY (Leave blank)	2. REPORT DATE	3. REPORT TYPE AND DATES COVERED
		FINAL REPORT 01 Apr 95 - 31 May 97

4. TITLE AND SUBTITLE
Hysteresis and Acoustic Emission as Non-Destructive Measures of The Fatigue Process in Metals

5. FUNDING NUMBERS
61102F
2305/GS

6. AUTHOR(S)
Dr S. A. Guralnick

7. PERFORMING ORGANIZATION NAME(S) AND ADDRESS(ES)
Dept of Civil and Architectural Engineering
Illinois Institute of Technology
3200 South State Street
Chicago, Illinois 60616-3793

8. PERFORMING ORGANIZATION REPORT NUMBER

9. SPONSORING / MONITORING AGENCY NAME(S) AND ADDRESS(ES)
AFOSR/NE
110 Duncan Avenue Suite B115
Bolling AFB DC 20332-8050

10. SPONSORING / MONITORING AGENCY REPORT NUMBER
F49620-95-1-0288

11. SUPPLEMENTARY NOTES

12a. DISTRIBUTION / AVAILABILITY STATEMENT
APPROVED FOR PUBLIC RELEASE: DISTRIBUTION UNLIMITED

12b. DISTRIBUTION CODE

13. ABSTRACT *(Maximum 200 words)*

Piezomagnetic effects are due to interactions between the mechanical and magnetic mesostructure of materials. In particular, under repeated loading cycles, microplastic processes generate dislocations and modify the texture of grains, voids, inclusions, and other defects. These mechanical changes in turn alter the arrangement of the coextensive ferromagnetic domain structure and affect the intensity of the associated magnetic fields.

14. SUBJECT TERMS	15. NUMBER OF PAGES
FATIGUE, PIEZOMAGNETISM, HYSTERESIS, NON-DESTRUCTIVE EVALUATION, ACOUSTIC EMISSION	75
	16. PRICE CODE

17. SECURITY CLASSIFICATION OF REPORT	18. SECURITY CLASSIFICATION OF THIS PAGE	19. SECURITY CLASSIFICATION OF ABSTRACT	20. LIMITATION OF ABSTRACT
UNCLASSIFIED	UNCLASSIFIED	UNCLASSIFIED	UL

Illinois Institute of Technology
Chicago

Type: Final Technical Report

Period: 1 April 1995 through 31 May 1997

Grant No: F49620-95-0288

Ora No: 4636-1-495861

IIT Report No: 5-54249-FR

HYSTERESIS AND ACOUSTIC EMMISSION AS NON-DESTRUCTIVE MEASURES OF THE FATIGUE PROCESS IN METALS

Sponsored by
The Air Force Office of Scientific Research

S.A. Guralnick
Principal Investigator
Investigator

T. Erber
Co-Principal

EXECUTIVE SUMMARY

It is well known from numerous experiments that repetitions of conventional fatigue tests with nominally identical specimens, carried out under carefully controlled conditions which replicate the loading programs as closely as possible, still lead to a significant scatter in the number of cycles to failure (N_f) that may exceed ±50%, These fluctuations originate from material differences in texture and structure at the mesoscopic level which cannot be eliminated by current fabrication techniques. Furthermore, detailed statistical analyses of patterns of microcrack propagation show that the fatigue process is extremely sensitive to slight variations in the initial states of the specimens, and that these differences are amplified by the repetitive application of external loads. Under these circumstances, the only means for improving the prediction of fatigue life is to identify some indices of performance in the early loading response of a particular specimen that forecast the expected value of its service life, N_f. Experiments show that this approach is feasible because the changes of the internal structure of a material subjected to repeated loading cycles are reflected in variations of the shapes and positions of the corresponding stress-strain hysteresis loops.

Some representative results are given in this report.

The three principal stages of fatigue---initial accommodation, accretion of damage and terminal failure---are clearly marked by the common transitions at cyclic history points N_2 and N_3. N_2 marks the 'end-of-the-beginning', and N_3 indicates the 'beginning-of-the-end! The detailed procedures that have been developed to identify the transition points are described in the body of the report. Comparisons among many experiments with similar steel specimens show that although the specific N_2 and N_3 values may fluctuate widely from run to run, the ratios $N_2/N_f \cong 12\%$ and $N_3/N_f \cong 92\%$ tend to be stable. This invariance implies that the mesoscopic state of the material at the end of the accommodation stage N_2, together with the loading program, essentially determines the terminal failure at N_f, even though in general $N_2 << N_f$. The net result is that the fatigue behavior of any particular specimen follows a predictable course regardless of the vagaries in its initial preparation or in its initial state.

Since fatigue is the cumulative result of material changes at the

mesoscopic level, phenmenological continuum variables such as total stress give an incomplete description of damage inception and organization. For this reason our instrumentation includes acoustic emission sensors and fluxgate magnetometers that can detect 'discontinuous' response to mechanical deformations. But, in a strict sense, identifying "jumps" with discontinuous behavior can be misleading. What the measurements described in this report show is that when variables such as magnetization or strain evolve in time, incremental changes may be concentrated in very small intervals. The corresponding mathematical idealizations are functions that have finite total fluctuations on arbitrarily small intervals---that is, they are not absolutely continuous. Functions of this type are useful for describing the intermittent accretion of mesoscopic damage because they may be strictly monotonic and yet have vanishing derivatives.

It has been found that there are distinct piezomagnetic effects which correspond to mesoscopic changes in the material which occur during the three principal stages of fatigue. Results from simultaneous measurements of magnetic field (B), stress (σ) and strain ($\in$) made upon steel specimens subjected to cyclic loading are given in this report. These measurements

give further evidence that the fatigue process proceeds through three distinct stages: initial accommodation, accretion of damage and terminal failure. Furthermore, these three stages are characterized by discernable cycle-by-cycle changes in the stress (σ) –field (B) and strain ($\in$) –field (B) hysteresis loops. There may well be far-reaching implications for the prediction of the fatigue behavior of metals from these new results.

PIEZOMAGNETISM AND FATIGUE

Abstract

Piezomagnetism refers to a change in the intrinsic magnetization of a material subjected to mechanical actions such as tension or compression. In a ferromagnet such as a mild steel these effects are large and easily measured: typically a stress of 2×10^4 lbs/in^2 or 140 MPa induces a magnetic moment of the order of 5×10^{-3} emu or 5×10^{-6} Am^2. The resulting flux densities in the vicinity of the specimen are then in the range 10 mG or 1μT; field variations of this magnitude can be accurately monitored by fluxgate magnetometers. Piezomagnetic effects are due to interactions between the mechanical and magnetic mesostructure of materials. In particular, under repeated loading cycles, microplastic processes generate dislocations and modify the texture of grains, voids, inclusions, and other defects. These mechanical changes in turn alter the arrangement of the coextensive ferromagnetic domain structure and affect the intensity of the associated magnetic fields.

Since fatigue is the cumulative result of the accretion of damage and the coalescence of microcracks, the progressive degradation of materials under cyclic loading can be tracked by following the evolution of the piezomagnetic field. Specifically, if the measurements are displayed as loci in a three-dimensional stress (σ) – strain (ϵ) – field (B) space, the approach to fatigue failure is paralleled by a series of conspicuous geometric transformations of these curves. Complementary information also appears in continuous-time records of B(t): these magnetograms clearly show the abrupt incidence of 'infarcts' (microcracks) and the cumulation of phase shifts as the material degrades.

1. Magnetomechanical Effects

There are widespread efforts both in industrial environments and in basic research laboratories to detect the destructive progression of fatigue processes in materials by utilizing a variety of magnetomechanical interactions. These effects can be divided into four broad generic classes:

(1) Magnetostriction is a geometric distortion of a material that occurs in response to the application of magnetic fields [1]. In conventional ferromagnets such as iron the relative

length changes or strains induced by weak external fields of the order of 10 Oe or 800 Am^{-1} are rather small, falling into the range $\Delta l/l \sim 10^{-6}$. But specially tailored materials such as the rare-earth alloy Terfenol-D ($Tb_{.3}$ $Dy_{.7}$ Fe_2) can exhibit magnetic dilations as large as $\Delta l/l \sim 10^{-3}$ [2]. Since these effects are the result of a set of complex interactions between the mechanical (grains) and magnetic (domains) mesostructure of materials, they are generally non-linear, irreversible, and history dependent. In particular, magnetostriction in iron and steels is non-monotonic --- diminishing in external fields exceeding 20-40 Oe --- and exhibits a cycle-dependent or drifting hysteresis [3-6]. Similar complications appear in the inverse effect:

(2) Piezomagnetism is the generation of magnetization by mechanical means. It was originally exploited in the old art of 'stroking' pieces of iron to make permanent magnets [7]; and it is still an inadvertent nuisance when steel tools are jumbled together. Another observation growing out of practical experience is that fields as large as 30 Oe appear on the fresh fracture surfaces of unmagnetized mild steel bars that fail in tension. The first systematic investigations of piezomagnetic effects were carried out by Villari around 1864-5 [8]. The instruments available at that time restricted his measurements to correlating transient flux changes in iron and steel rods with sequences of blows, tugs, and twists. But some inferences concerning static relations could be deduced by superposing steady magnetic fields and applying constant tension. The principal results are that in iron

and steel tension produces an increase in magnetization in weak fields and a decrease in strong fields. The locus of these cross-over points, or Villari reversals, tends to decrease with increasing tension[4,5]. This non-monotonic response and the associated drifting hysteresis mirrors the behavior of the corresponding magnetostrictive effects.

(3) Since it is experimentally difficult to obtain a clear separation between effects induced solely by either mechanical or magnetic means, most of the research literature deals with the **cross-modulation** produced by the joint action of externally imposed stresses and magnetic fields. For instance, some non-magnetic austenitic steels undergo a strain-dependent transformation to a ferromagnetic martensitic phase. The resulting magnetization can then be determined with the aid of a Hall probe - permanent magnet assembly, and calibrated to yield the value of the peak strains [9,10]. Effects corresponding to the Villari reversals occur when constant magnetic fields are applied while tension is continually increased: In materials such as iron and permalloys the magnetization increases until the elastic limit is reached, and thereafter decreases as plastic deformations alter the domain structure. The threshold of plastic flow also enhances the changes in magnetization that occur before and after the application of cyclic stress [11]. Similarly, tension and compression alter the shapes of magnetic hysteresis loops [12-20]; these effects are used in non-destructive evaluation (NDE) [21-23]. Other variants related to magnetostriction concern changes in Young's modulus, E: When some ferromagnetic

materials are stressed, the primary elastic response is perturbed by magnetostrictive dilations due to reorientations of the domain structure. The fractional changes in the effective modulus can be quite large, $\Delta E/E \sim 10^{-3}$ to 10^{-1}; and may be influenced by applying variable magnetic fields [4]. Measurements of these effects show considerable scatter among different specimens, as might be expected for structure-sensitive properties[5].

(4) A qualitatively different set of phenomena appear on refined scales of measurement: **'Discontinuous' magnetomechanical effects** are the direct result of mesoscopic transformations in materials. For instance, when the stress on a macroscopic solid is continuously varied by hydraulic means, the yielding reponse is generally also smooth, but occasionally interrupted by minute length jumps of the order of 10^{-5} cm. These Portevin - Le Chatelier discontinuities occur on time scales as short as 10^{-6} s, and presumably are due to the intermittent locking and slipping of microstructural elements such as grains or crystallites [24-26]. With scanning tunneling microscopes this step-like behavior can be followed down to strains as small as 10^{-8} [27]. On a still finer scale, sudden microstructural rearrangements can also be detected by acoustic emission techniques. Typically, ultrasonic pulses in the band around 300 kHz with total energies as low as 10^{-24} J or 6×10^{-6} eV can be distinguished from the thermal phonon background [28]. The magnetic counterpart of these effects is Barkhausen emission [29]. If a ferromagnetic material is subjected to variable magnetic fields or stresses some of the magnetic domains

respond by abrupt shifts of their configurations on a time scale < 10^{-3} s. The associated magnetization changes then result in a sequence of jumps in the ambient field.

Magnetization steps as small as 10^{-8} emu, or 10^{-11} Am^2, corresponding to volume rearrangements of the order of 10^{-11} cm^3 , can be detected by superconducting fluxmeters (SQUIDs). Several variants of these mechanical and magnetic discontinuities may occur simultaneously. For instance, magnetostrictive length jumps of approximately 10^{-7} cm have been observed in coincidence with Barkhausen signals from nickel wires [30]. Similarly, intermittent crack movements in stressed ferromagnets can generate simultaneous magnetic and acoustic pulses [31]. Because of their refined stress sensitivity, these effects have been incorporated into several commerically available NDE instruments [32-38]. The response of these devices can be related to the integrity of materials and structures by means of two general empirical trends: (*i*) Very low level stress or field cycles tend to remove discontinuities. If the amplitudes of these cyclic excursions are slowly increased, the range of diminution of acoustic and/or Barkhausen emission is extended and 'remembered' from cycle to cycle [28,39-41]. At still higher field or stress levels, this Kaiser effect disappears and is replaced by a regime of steady hysteresis accompanied by persistent acoustic and/or magnetic ermission. (*ii*) If the cyclic stresses are sufficient to cause eventual fatigue failure, the cumulation of material damage is reflected in the variation of the acoustic and magnetic signals. These are generally very high during the first and second cycles of load application, and decrease by an order of

magnitude during the initial 10%-20% duration of life. Fatigue experiments also indicate that acoustic emission levels rise drastically during the last 10% of load cycles before final rupture.

In a strict sense, identifying jumps with discontinuous behavior is misleading. What the measurements actually show is that when variables such as magnetization or strain evolve in time, incremental changes may be concentrated in very small intervals. The corresponding mathematical idealizations are functions that have finite total fluctuations on arbitrarily small intervals---that is , they are not absolutely continuous. Functions of this type are useful for describing the intermittent accretion of mesoscopic damage because they may be strictly monotonic and yet have vanishing derivatives [42].

2. Piezomagnetism as an Indicator of Fatigue

It is apparent from the preceding summary that the intrinsic variability of many magnetomechanical effects is due to their history-dependent evolution from initial states whose mesoscopic structures cannot be reproducibly controlled. The essential point of using piezomagnetism to monitor the progression of fatigue is to turn this vice into a virtue. It is well known from numerous experiments that repetitions of fatigue tests with nominally identical specimens, carried out under carefully controlled conditions which replicate the loading programs as closely as possible, still lead to a significant scatter in the number of cycles to failure (N_f) that may exceed ±50%. These fluctuations originate from

material differences in texture and structure at the mesoscopic level which cannot be eliminated by current fabrication techniques. Furthermore, detailed statistical analyses of patterns of microcrack propagation show that the fatigue process is extremely sensitive to slight variations in the initial states of the specimens, and that these differences are amplified by the repetitive application of external loads [43]. Under these circumstances, the only means for improving the prediction of fatigue life is to identify some indices of performance in the early loading response of a **particular** specimen that forecast the expected value of its service life N_f . Experiments show that this approach is feasible because the changes of the internal structure of a material subjected to repeated loading cycles are reflected in variations of the shapes and positions of the corresponding stress-strain hysteresis loops. Some representative results are illustrated in Fig. 1. The upper trace shows the variation of the hysteresis loop areas, or energy dissipation $\Delta U(N)$, as a function of the number of loading cycles N. The lower trace shows the variation of another index, the hysteresis loop distance $D\{\ell(1); \ell(N)\}$, which is a quantitative measure of the changes in shape and position of the stress-strain loci between cycles 1 and N [44-46]. The three principal stages of fatigue---initial accomodation, accretion of damage and terminal failure---are clearly marked by the common transitions at N_2 and N_3. Comparisons among many experiments with similar steel speciments show that although the specific N_2 and N_3 values may fluctuate widely from run to run, the ratios $N_2/N_f \cong 12\%$ and $N_3/N_f \cong 92\%$ tend to be stable. This invariance implies that the mesoscopic state of the material at the end of the accomodation stage N_2, together with the loading

program, essentially determines the terminal failure at N_f, even though in general $N_2 << N_f$. The net result is that the fatigue behavior of any particular specimen follows a predictable course regardless of the vagaries in its initial preparation.

Since the variations of piezomagnetic effects in ferromagnets depend both on the mechanical and magnetic microstructures, it might seem that the uncertainties concerning the initial states of the materials would be compounded. Indeed, even the simplest situation, the nature of the demagnetized state, is a matter of controversy [47]. The basic point is that vanishing magnetizations---on gross spatial scales averaged over many domains---can result only from highly ordered patterns in which the magnetic moments of the individual domains cancel. These unmagnetized states cannot be produced by the usual expedient of randomizing the domain structures with fluctuating external fields that are slowly turned off. Experience with erasure and noise on magnetic tapes, as well as specialized experimental studies, confirm that the lower limits of magnetization ($|\vec{M}|_{demag}$) attained by conventional demagnetization methods are equivalent to adding the moments of the individual domains ($\vec{\mu}_{dom}$) by a 'random-walk' estimate, i.e.,

$$|\vec{M}|_{demag} \sim < |\Sigma\, \vec{\mu}_{dom}| > \sim (8n/3\pi)^{1/2} < |\vec{\mu}_{dom}| > \qquad (2.1)$$

where n is the number of domains in the sample [41]. In the case of steel, where single magnetic domains have volumes of the order of 10^{-10} cm^3 and moments of 10^{-7} emu,

eq. (2.1) indicates that a demagnetized test piece with an effective volume of 1 cm^3 will have a residual moment in the range $|\vec{M}|_{demag} \sim 10^{-2}$ emu or 10^{-5} Am^2. Consequently, any nominally demagnetized bulk steel sample will have an ambient background field of the order of O.1G or 10μT within 1 cm of its surface. This 'universal' magnetic halo is analogous to the 10^{-6} Vm^{-1} electric fields that surround all conductors in the earth's gravitational field [48-50]. In the absence of shielding, this O.1G residual field is negligible compared to the earth's field and---in practical fatigue trials--- the stronger background fields (~1 G) associated with the massive test machinery. However, since the coercivity of steels usually exceeds 20 Oe or 1.6 kAm^{-1}, and the demagnetizing factors of the fatigue specimens are approximately 0.5, the background fields are too weak to significantly perturb the demagnetized states.

The parallel development of piezomagnetic effects and the stages of fatigue indicated in Fig.1 can now be followed in greater detail. Suppose that initially a steel specimen is demagnetized so that its magnetic state is at the zero point of the anhysteretic magnetization curve [5]; then in accordance with eq. (2.1), this also corresponds to a state of optimum domain disorder. Since steel has a magnetocrystalline energy density K of the order of 10^5 erg cm^{-3} or 10^4 Jm^{-3}, and a Young's modulus $E=29.6\times10^3$ ksi $\cong 2\times10^{12}$ ergs cm^{-3}, even low levels of strain such $\in \cong 6\times10^{-4}$ are sufficient to raise the stored elastic

energy density $\mathcal{E}_{el} = E\epsilon^2/2$ to the point where $\mathcal{E}_{el} > K$. When this energy parity is reached, the magnetic domain structures will be altered by mesoscopic stress fields, and systematic field variations will be superposed on the random initial field given by (2.1). In typical fatigue experiments with steel where the peak stress ranges may be 100 ksi or 70 kg mm^{-2}, the corresponding flux variations at distances of about 1cm from the specimens will be approximately 25 mG or 2.5 μT. Assuming very conservative sensitivity and stability limits of $\pm$ 1 mG for fluxgate magnetometers, it is in principle possible to detect the reorientation of as few as 10^{16} iron atoms. The aggregate equivalent volume of this number of atoms is about 10^{-7} cm^3, or roughly comparable in size to a steel grain or microcrack.

Both traces in Fig.1 show that the stress-strain response of fatigue specimens varies drastically during the initial cycles of loading, and then relaxes to a more gradual rate of change. This transition also appears in acoustic emission--the number of detected pulses or 'hits' generally decreases by an order of magnitude from the first to the second cycle, and ultimately tends to level off in the vicinity of N_2. Similarly, the piezomagnetic field patterns change conspicuously during the first few cycles; and the associated Barkhausen noise also tends to diminish [33,34]. All of these effects are consistent with a progressive accomodation of the materials' internal stress distribution to the cyclic loads. Model simulations with elastic-plastic frameworks show that below a critical load level---

the 'shakedown load'--- the cyclic stress patterns shift so that eventually the entire system responds elastically; whereas for larger loads this compensation remains incomplete, and plastic deformations occur during every cycle [44,51,52]. The corresponding critical load in fatigue is the endurance or fatigue limit σ_{fl}. If, as in Fig.1, the external loading exceeds this limit (i.e., $\sigma/\sigma_{fl} \sim 2$), the optimum material accomodation occurs in the vicinity of N_2, but is not sufficient to suppress all microplastic flows. Consequently, every succeeding cycle in the accretion range $N>N_2$ will generate additional damage.

The average stress-strain hysteresis loop area $<\Delta U>$ in Fig.1 is equivalent to 1.1 kip-in/in^3 or 7.5×10^7 erg cm^{-3}. Nearly all of this energy is dissipated in heat, and less than 1% is retained as damaging energy per cycle, $<\Delta U_d> \sim 6\times10^5$ erg cm^{-3}. This disparity shows why it is so difficult to obtain direct information concerning fatigue damage from the averaged properties of 'stabilized' stress-strain hystersis loops. According to several independent estimates, the energy associated with the development of an elementary defect in the material is of the order of 3 eV [44,53]. Therefore $<\Delta U_d>$ is equivalent to the creation of about 10^{17} defects per cm^3 during every loading cycle. If each of these defects in turn modifies the orientation of a single Bohr magneton ($\mu_B \sim 10^{-23}$ Am^2), then the preceding estimates indicate that the aggregate magnetization changes could lead to field variations in the 1 to 10 mG range at the fluxgate probes. Fluctuations of this order of magnitude are in fact observed experimentally.

The complementary role of magnetic and mechanical measurements during the lengthy accretion stage between N_2 and N_3 should now be clearer. As damage accumulates, the mesostructure of the material is altered, and this modifies the shapes of the associated stress-strain hysteresis loops. By comparing quantitative measures of the hysteresis drift, such as the loop distance $D\{\ell(N_i); \ell(N_j)\}$, over sufficiently long cycling intervals---e.g., $|N_j - N_i| \sim \mathcal{O}(N_f^{1/2})$---the secular increase in damage can be reliably distinguished from the dominant effects of heat dissipation. In contrast, the tremendous sensitivity of magnetometers permits direct measurements of the cycle-by-cycle changes in the stress (σ) - field (B) and strain ($\in$) - field (B) hysteresis loops. Basically these variations are due to the stress-induced formation of dislocations, slip bands, Lüder's lines, microcracks, and other mesoscopic structures incorporating 10^6 or more atoms [54]. The associated organized grouping of magnetic moments partially replaces the disordered domain patterns remaining from the initial demagnetization, and these coherent field increments alter the σ- B and $\in$-B hysteresis loops. However, since the net effect of combining magnetic structures can be either to increase or decrease the overall magnetization [47], there are no simple monotonic correlations between the accretion of damage and magnetic field amplitudes.

The rapid variations of the mechanical, acoustic and magnetic indices that occur during the terminal stage of fatigue between N_3 and N_f in Fig.1 mirror the swift pace of change during the initial accomodation,$N< N_2$; but, of course, the underlying processes are quite different, and the end result is rupture rather than stabilization. Detailed analyses of

many traces, such as those in Fig. 1, show that the transition at N_3 corresponds to a change from linear to exponential behavior. In this particular example $N_3/N_f \cong 90.6\pm$ 0.7%, which yields a terminal failure interval of $N_f - N_3 \cong 139\pm 10$ cycles. The largest piezomagnetic effects are concentrated in the last few milliseconds of the final cycle when the steel samples fail in tension. Total flux changes of approximately 0.3 Wbs^{-1} or $3x10^7$ Mxs^{-1} are associated with the inception and propagation of the terminal crack [55,56]. After rupture, the fracture surfaces of the specimens exhibit gross fields of the order of 30 G.

3. Experiments

The principal components of the fatigue test system are shown in Fig.2. Two electronically controlled MTS-810 servo-hydraulic testing machines with peak capacities of 22 kips or 97.8 kN and 50 kips or 222 kN are available for applying cyclic tension and compression. The solenoid valves and pumps for both machines are located remotely to minimize acoustic and electromagnetic interference. Accurate mounting of the fatigue specimens is facilitated by hydraulic collet grips. The loading sequences are programmed on type 458.20 microconsoles. As indicated by the microprofiles in Fig.2, most of the fatigue tests were run under strain control using symmetric triangular waveforms. Low cycle fatigue tests that could be completed in a single day ($N_f \cong 6000$) were generally carried out with slow ramping rates set at 10s for a complete cycle; the longer runs had periodicities of 2s per cycle. Load values were derived from a type 661.20 E - 03 force

transducer with a non-repeatability limit of 0.03% full scale. The corresponding strains were measured with a type 632. 13E-20 extensometer mounted directly on the specimens. Over a maximum strain range of ± 0.15, the hysteresis and non-linearity of this gauge are 0.10 % and 0.15% respectively. The knife edges that sense the displacements are separated by 0.500 in.; this provides adequate clearance for the acoustic and magnetic sensors. Electromagnetic interference from the extensometer is minimized by low internal bridge currents (< 1 m A near balance), aluminum construction, and shielded leads.

All of the fatigue specimens were machined from a single bar of cold finished unannealed AISI 1018 steel to the dimensions shown in Fig.2. Axial tension tests on a series of ten specimens yielded the following mechanical properties:

elastic modulus (E)	30×10^3 ksi	210 GPa	
proportional limit (σ_{pl})	48 ksi	330 MPa	(3.1)
yield strength (0.2% offset) (σ_y)	71ksi	490 MPa	
ultimate tensile strength (σ_u)	78ksi	540 MPa	

The rms scatter of these results was about 2.3% without any noticeable outliers. In contrast, fatigue trials with carefully finished and polished test pieces occasionally yielded cycles-to-failure (N_f) variations as large as 100%. All of the values listed in (3.1), as well

as the results of chemical analyses, are consistent with the usual specification for AISI 1018 steel.

Magnetic signals were detected by fluxgate magnetometers (HP 3529A/428B and APS 460/428C). These instruments have several features that match the requirements of the piezomagnetic measurements: (1) The field ranges that can be measured --- 0.1 mG to 10 G --- include all of the relevant effects: the background fields (~ 1G); the field variations of the piezomagnetic hysteresis loops (1 to 30 mG); intermittent field excursions due to cracks (~100 mG); and incremental field changes accompanying fatigue (0.1 to 5 mG). (2) The compact cylindrical form of the fluxgate probes --- 0.27 in. OD --- allows them to fit between the extensometer knife edges so that they almost touch the fatigue specimens (Fig.2). In this position, the distance between the center of the axial flux sensing element and the metal surface is only about 12mm. The zone of maximum fatigue damage therefore also coincides with the region of optimum probe sensitivity. Auxiliary measurements confirm that the fields originating from the ends of the specimens and the hydraulic grips are attenuated by an order of magnitude. (3) This spatial discrimination is sharpened by the axial probe construction. Only the field component parallel to the cylindrical axis of the sensing element is measured. Specifically, with reference to Fig.2, this means that increasing magnetometer (current) readings correspond to increasing field values when $\vec{B}$ points from the speciment to the probe. Since piezomagnetism basically

results from the interaction of material deformations, described by a second order strain tensor, with a vector field, a complete determination of all 18 phenomenological coupling constants would, in principle, require measurements of all components of $\vec{B}$. However, currently available 3-axis fluxgate probes are too bulky to integrate with the fatigue test set-up. (4) The combined noise and short-term drift of the magnetometers is approximately 10 μG peak-to-peak. This stability and the robust operating characteristics of the fluxgate instruments are essential for the fatigue measurements. Long runs can extend over several days, but the occurrence of isolated events during individual cycles --- persumably correlated with crack formation or crack advance --- requires that all of the sensors function continuously throughout the test.

Since most of the crucial fatigue measurements depend on quantifying the changes in successive hysteresis loops, it is convenient to use the initial cycle as a reference. Figure 1 illustrates this situation for stress-strain hysteresis. A similar starting point for the piezomagnetic measurements can be obtained by nulling out the background fields due to the earth and the test machinery, as well as the residual fields of the demagnetized specimen (2.1). In practice, as shown on the inset in Fig.2, this compensation was managed with a small 500 turn air-core coil positioned near the fluxgate probe. Depending on the precise orientation of the coil and probe, approximately 50 mA supplied by a constant current source was sufficient to reduce the magnetometer reading to 2 mG. The sensitivity of this arrangement could be increased to about 25μG per mA. An

alternate compensation scheme that also worked involved the use of a linear array of four stabilized Cunife I magnets [57]. In fact, this was the first method tried in the initial piezomagnetic fatigue experiments.

Several precautions are necessary to ensure the stability of the magnetic reference field and to avoid spurious effects: (*i*) The magnetometer probes and compensating devices should be fixed in position by rigid non-magnetic supports which are decoupled from all mechanical flexures of the test stand. (*ii*) Any magnetic field variations originating from the hydraulic grips, the electronic controls of the MTS-810 materials testing system, or other ambient sources should be separated from the piezo-fatigue effects by continuous monitoring with auxiliary magnetometers placed in 'guard' positions. *(iii)* If the field compensation is maintained by coils, any current 'glitches' that could counterfeit magnetization jumps in the fatigue specimen should be identified and recorded. Unfortunately, due to lack of adequate computing power, it was not found to be feasible to implement all the measures in (*ii*). But periodic checks, including trials with non-magnetic specimens, indicated that the piezomagnetic data was not corrupted by spurious effects. Similar limitations apply to the current monitoring in (*iii*). This problem was partially detoured by using permanent magnets and substituting vigilance for automatic control.

Previous experience has shown that acquiring fatigue data at a rate of 100 samples per cycle provides reasonable accuracy without overloading the computer system[44]. With the expanded set-up in Fig. 2, this implies recording values of the time (t), strain (ϵ), stress (σ), and field (B) every 20 ms during a complete two second loading cycle. Even for a very short run of about two thousand cycles, this requires the storage and manipulation of data sets comprising several million numbers. As indicated by the block diagram in Fig. 2, the mechanical and magnetic signals were transmitted to the data acquisition computer through a DT 756 interface connecting board and a DT 2801 data translation coprocessor. Off line data analysis was carried out by separate computers. Acoustic emission signals were detected by a 150 kHz piezoelectric sensor (R15/c) and processed by a Locan 320 system.

4. Results

When a steel specimen is subjected to a symmetric triangular strain cycle---following the microprofiler trace in Fig. 2---the general piezomagnetic response is a hysteresis locus in a three-dimensional space whose coordinate axes represent strain (ϵ), stress (σ) and magnetic field (B). This locus is the irregular curve shown in the central box in Fig. 3. The little fold-out guide in the lower right hand corner relates this three-dimensional hysteresis response to the three two-dimensional projections that surround the central box. The top projection corresponds to the standard stress-strain hysteresis loop

that is obtained in conventional mechanical measurements. It is remarkable that this simple lozenge shape is actually the 'shadow' of a much more complicated curve in a three-dimensional space. The double points that appear in the two side projections--- corresponding to stress-field and strain-field hysteresis traces--- indicate the complexity of this curve. Figures 4(a) and 4(b) show rotated and enlarged views of the ϵ-σ-B locus measured at 100 successive points during a complete strain cycle. Obviously, in these three-dimensional representations, all the variables are single-valued functions of the time. It is only when the convolutions near the 'heads' and 'tails' of these duck-like curves are projected into the ϵ-B and σ-B planes that the resultant traces may include double points.

The basic connection between piezomagnetism and fatigue is summarized in Fig. 5. The solid line is the locus of Fig. 4(a) displaying the magnetomechanical behavior of the specimen during the initial stage of fatigue cycling ($N/N_f \cong 2.7\%$): the dashed line is transposed from Fig. 4(b) and shows the response during the late stage of fatigue ($N/N_f \cong 92.4\%$) just prior to the onset of terminal failure. Clearly there are marked changes both in the shape as well as the position of the locus reflecting the cumulative modifications of the material's internal structure.

The progression of fatigue is shown is still greater detail by the sequence of panels in the next set of illustrations: Fig. 6(a) displays eight consecutive strain - field hysteresis

traces corresponding to the left projection in Fig. 3. Since the fold-out in Fig. 3 reverses the direction of increasing strain, all the 'ducks' in Fig. 6(a) face in the opposite direction. Superficially every member of this gaggle looks alike. But even in the compressed format of these illustrations it is easy to verify that every trace is actually different: For instance, the double-pointed 'tail' in cycle 10 is higher than in cycle 9; the 'back' in cycle 11 has a different contour than in cycle 10; a second double-point has developed in the 'beak' of cycle 12; this feature temporarily disappears in cycle 13; and an overlay of cycle 14 and cycle 11 shows a complete mismatch of the two traces. These distinctions are even more conspicuous in the evolution of the stress-field hysteresis traces. Figure 6(b) displays eight consecutive hysteresis cycles matching the sequence in Fig. 6(a). The pairing of these orthogonal views is illustrated in Fig. 3. To be precise, cycle 10 in Fig. 6(a) is a front projection---in the ϵ-B plane---of the three-dimensional locus in Fig. 4(a), and cycle 10 in Fig. 6(b) is a side projection--- in the σ-B plane---of this same three-dimensional locus. It is evident that the shape of the 'ducks' heads in Fig. 6(b) change drastically from cycle to cycle. Since the corresponding peak stress levels lie between the material's proportional limit and the yield strength, cf.(3.1), it is plausible that the maximum magnetic effects are correlated with the region of greatest plastic deformation. Similarly it is reasonable to identify the downward tilt of the 'heads' with the Villari reversals discussed in Section 1. In contrast, the shape and positions of the ducks' tails---coinciding

with the region of maximum compressive stress--- tend to remain relatively stable.

Figure 6(c) shows the corresponding sequence of stress-strain hysteresis loops for cycles 9 through 16. The point of basic interest here is that the consecutive mechanical hysteresis traces essentially coincide even though the associated magnetic hysteresis traces vary perceptibly from cycle to cycle. Since the mechanical measurements have a precision of approximately 0.2%, these disparities between the magnetic traces in Fig. 6(a) and 6(b), and the mechanical traces in Fig. 6(c), are not merely due to mismatches in amplifier gain settings, but rather are consequences of inherent differences in the sensitivities of piezo-magnetic and mechanical responses to the progression of fatigue. Of course, more refined analyses can detect the evolution of fatigue through gradual changes in the stress-strain hysteresis curves. In particular, Fig. 7 shows the variation of the hysteresis energy (density) dissipation $\Delta U(N)$ as a function of the number cycles N for the fatigue experiment corresponding to Figs. 4(a) to 6(c). The general form of this curve closely resembles the canonical shape of the dashed trace in Fig. 1: This comparison shows that cycles 9 through 16 in Figs. 6(a) to 6(c) are part of the initial accommodation stage of the fatigue process. In fact, the adjustment to the external stress cycles in so rapid that the difference between $\Delta U(9)$ and $\Delta U(16)$ is only about 1.5%; this change is too small to be noticeable among the hysteresis loops in Fig. 6(c).

According to Fig. 1, the next region of interest in the fatigue process is the transition from the accretion of damage to terminal failure in the vicinity of N_3. In the present instance, Fig. 7 shows that this transition occurs during cycles 330 to 355. Some details of the associated piezomagnetic changes are displayed in the eight consecutive strain-field hysteresis traces in Fig. 8(a). It is obvious that the duck shaped curves in Fig. 6(a) have been severely distorted, and the pace of cycle-to-cycle changes continually accelerates. The most prominent trend is the increasing droop and undulating contour of the successive 'bellies'. As indicated by the arrows in cycles 338 and 339, these features appear during the decreasing part of the strain cycle: The flatter segments, marked by the arrows in cycle 340, are traced out while the compressive stress increases from 16 to 46 ksi. In the vicinity of maximum compression (~ 60 ksi) and minimum strain, the ducks' heads of Fig. 6(a) have turned into long narrow beaks with varying numbers of double points: furthermore, the earlier increases in field---indicated by the arrow in cycle 9 of Fig. 6(a) --- have evolved into the downward sloping beaks of Fig. 8(a).

These general changes in shape are also evident if the stress-field hysteresis curves in Fig. 6(b) are compared with their counterparts in Fig. 8(b). For instance, the arrows in cycle 9 and cycle 337 have very different slopes, and the associated ducks' tails in Fig. 8(b) are systematically higher than those in Fig. 6(b). In quantitative terms, this means that at the point of maximum compressive stress, the steel's magnetization has increased by a factor of approximately 1.25 as a result of the effects of fatigue. A

summary of all of these changes is given in Figs. 9(a) - 9(c). Each panel overlays a solid hysteresis curve acquired during the early stage of fatigue (cycle 10) on a dashed hysteresis curve obtained during the late stage (cycle 340). These three views are orthogonal projections of the three-dimensional hysteresis loci in Fig.5. Clearly the progressive alterations of the material's mesostructure during the development of fatigue are reflected in conspicuous changes in the the piezomagnetic hysteresis. In particular, the contrasts between Figs. 9(a) - 9(b) and Fig. 9(c) suggest that in multidimensional hysteresis the projections with greater complexity are more sensitive indicators of changes in the underlying physical processes than the projections that yield simpler curves. It is possible that rotations about the B-axis in Fig. 5 could lead to other projections furnishing even more refined information.

Figure 1 and Figure 7 both show that terminal failure is a stage of relatively rapid change from cycle to cycle. The coalescence of defects and microcracks weakens the material to such an extent that it can no longer sustain tensile stresses, and therefore, as indicated in Fig. 9(c), the mechanical hysteresis loops tend to flatten and shrink. Figure 7 shows that this transition to catastrophic failure is straddled by cycles 345 to 355: the corresponding piezomagnetic transformations are illustrated in Fig.10. Obviously, the sharp down turn of the stress-strain hysteresis loop areas that begins at cycle 348 in Fig. 7

is correlated with severe distortions of the stress-field traces. While cycle 348 in Fig.10 is still recognizable as a continuation of cycle 344 in Fig. 8(b), all qualitative similarities have essentially been obliterated by cycle 354. The peak stress in cycle 344 is 58 ksi, and the corresponding magnetization range (max B/ min B) is approximately 3.5; in cycle 354 the peak stress is 38 ksi, and the magnetization range has decreased to 1.7. During the last few cycles, before the end of the of test at cycle 368 (N_f), the steel between the extensometer blades has been so severely degraded by damage, that it has a consistency analogous to stiff taffy. The strain-field response of this viscous ferro-fluid consist of irregular traces with little hysteresis. Two examples, obtained during cycles 357 and 367, are shown in Fig. 10. However, since the inception and organization of mesoscopic damage is stochastic, the coalescence of microcracks can also result in a fracture of the entire specimen. In this extreme, failure occurs at non-negligible levels of tensile stress, and the flux variations associated with final rupture have an entirely different character [55,56].

5. Results (cont.)

All the data summarized in Fig.4(a) - Fig.10 correspond to experimental conditions which were adjusted to amplify the correlations between piezomagnetic effects and the progression of fatigue. The peak tensile stresses reached 72 ksi or 496 MPa

which, as indicated in eq. (3.1) and Fig. 13 of reference [44], is comparable to the yield strength of the steel. Under these extreme conditions plastic deformations generate copious damage --- of the order of 5×10^{17} defects/cm^3 per cycle --- and the specimen fails after only 368 cycles. Furthermore, if the creation of every defect is associated with the reorientation of an iron atom, the total magnetization changes of the specimen could be as large as 3×10^{-3} emu per cycle. The corresponding field variations at the fluxgate probe would then be about 6 mG or 0.14 V; and, indeed, changes of this magnitude are clearly visible by comparing the piezomagnetic hysteresis traces with the ordinate scales of Figs. 6(a) - 6(b), and Figs. 8(a) - 8(b).

In most applications, the mechanical stresses are lower, and the number of cycles to fatigue failure (N_f) increases. The corresponding magnetic field variations from cycle-to-cycle are then of the order of $2.2\ N_f^{-1}$ G. If $N_f > 10^6$, as is usually the case in high cycle fatigue, these piezomagnetic field variations are nominally in the microgauss range. Detecting such small differences in successive hysteresis loops whose intrinsic field variations may be three or four orders of magnitude larger is difficult. An obvious solution, illustrated in Fig. 5 and Figs. 9(a) - 9(b), is to compare the hysteresis patterns from widely differing numbers of cycles. Figure 1 indicates that this approach is useful for estimating fatigue lives from cumulative changes in stress-strain hysteresis. In order to

identify similar indices of fatigue in piezomagnetic measurements it is convenient to display the data as a function of time. The three strip-chart cycles in Fig.11 partially overlap the data in Figs. 6(a) - 6(c), but show the correlations among the measurements in greater detail. Specifically, the top strip shows the triangular $\in$ - t profile of the strain controlled loading which was programmed into the testing machine. Since in this case the strain range, $0 \leq \in \leq 0.018$, is restricted to expansions, the corresponding hysteresis is 'one-sided' [44]. The vertical reference lines, labeled SR and SR(0), indicate the correlation of the strain reversals with the maximum tensile and compressive stresses in the bottom strip. The dashed line in cycle 12 shows the onset of non-linear behavior at the proportional limit at 48 ksi, cf. (3.1). The magnetic field traces in the middle strip are effectively fold-outs of the duck patterns in Figs. 6(a) - 6(b). As a result, ambiguities such as the double points in the ducks' tails in Fig. 6(a) are resolved into sequential pairs marked by the D - arrows. The correspondence of the field variations with strain reversals, the transitions through zero stress, and the onset of plastic flow are indicated by the series of SR, O, and P arrows.

Figure 12 shows the continuation of these strip charts about three hundred cycles later. In this format the piezomagnetic changes are not as evident as in the duck patterns of Figs. 6(a) - 6(b) and Figs. 8(a) - 8(b), but the effects of fatigue are unmistakable in the overlay of Fig. 13. Clearly the greatest magnetization changes occur in the vicinity of the SR(o) reference lines that join the points of zero strain reversal and maximum compres-

sion. On the other hand, the crossing of the solid and dashed magnetic traces near the O and P arrows indicates that the magnetizations associated with zero stress and the proportional limit may be relatively stable, i.e. recurrent, during the accretion of damage.

The strip charts in Fig. 14 are excerpted from another fatigue experiment that was stopped at 4716 cycles after a large surface crack appeared and the tensile strength of the specimen decreased rapidly. The top record shows four successive magnetic field traces obtained near the beginning of the test. Although the peak strains ($\epsilon \leq 0.009$) and stresses ($\sigma \leq 53$ ksi) are significantly smaller than in the benchmark experiment discussed above, the total magnetic field variations within a single cycle (~ 34 mG) are actually larger by a factor of about 1.5. Nevertheless, in contrast to the cycle-by-cycle hysteresis fluctuations that are so evident in Figs. 6(a) and 6(b), detailed comparisons show that cycles 193 - 195 are essentially exact repetitions to within the accuracy of the measurements (< 0.5 mG). This result in consistent with our prior (fatigue damage) estimate that under these conditions the cycle-to-cycle field variations would be of the order of $2.2/4716 \sim 4.7 \times 10^{-4}$G.

The second magnetic strip chart in Fig.14 shows the cumulative effects of fatigue after another 4165 cycles. Although the overall shape of the traces is similar in the earlier and later magnetic records, there are differences in the detailed features. In particular, the prominent magnetic field peak which coincides with the SR(0) strain reversals in cycles

193 -195 has gradually shifted so that by cycle 4361 it occurs about 21° ahead of the zero strain points. Of course, the most interesting event is the large field excursion during cycle 4363. If the field decrease below the normal minimum level --- equivalent to an 'excess' field variation of 55 mG --- is identified with the correlated reorientation of a group of iron atoms, then this piezopulse corresponds to a mechanical transformation extending over a volume of about 10^{-5} cm^3. This is a reasonable size scale for stage II microfracture [54]. The expanded traces in Fig. 15 show that a precursor had developed at the junction of cycles 4361 and 4362 --- this cleft is marked by the C - arrows in Figs. 14 and 15. But whatever triggered this 'mesoquake' at cycle 4363 is effectively quenched during the succeeding cycles. An overlay of 4364 - 4366 shows that the magnetic patterns are nearly identical; this regularity persists for another 40 cycles when there is a renewed burst of activity. Further comparisons of the 'before and after' responses show a mixture of changes and invariance; Obviously the shapes and relative phases of the magnetic peaks in Fig. 15 are quite different on either side of the 'infarct' at cycle 4363. But the regions between the two sets of F - F arrows in cycles 4362 and 4367 are identical down to the smallest discernible serration. At first sight it is also striking that the cyclic mechanical response in the bottom strip of Fig. 14 continues unaltered through cycle 4363. This invariance can also be checked in greater detail by comparisons of the stress-strain hysteresis loops for cycles 4360 and 4363. However, if the magnetic excursion at cycle 4363 is indeed associated with the formation of a crack with an area of the order of

6×10^{-4} cm^2, then the corresponding macroscopic stress change is only 0.2%; and this effect is just below the level of detectability. As indicated previously, this type of silent cumulation of damage at levels below 5×10^{-5} defects/atom per microcrack can be described by monotonic functions with vanishing derivatives [42].

The last set of strip charts in Fig.16 demonstrates that evolutionary changes in piezomagnetic signals are still easily measurable under conditions approaching high cycle fatigue. These records are excerpted from a strain controlled experiment --- programmed for a strain range of 0.0035 --- where the specimen failed at about N_f = 250,245 cycles. The total field variations are comparable to those observed in the preceding experiments, and are still approximately 50 times larger than any noise due to fluctuations in the laboratory environment (e.g. actuators in the MTS - 810 test stand, fan motors, etc.). Since even at these low strain levels --- in the proximity of the endurance limit $\in_{f\ell} \cong$ 0.0013 [44]--- the peak elastic energy density ($\sim 1.3 \times 10^7$ erg/cm^3) is still 30 times higher than the nominal value of the magnetocrystalline energy, the observation of piezomagnetic effects of this magnitude is plausible. However, since the corresponding rate of damage formation has decreased to about 10^{14} defects/cycle, the profiles of successive field traces are essentially indistinguishable. The cumulative effects of fatigue are evident in the progressive alterations of the field patterns over larger intervals of cycles. For instance, the field minima, indicated by the M - arrows in the various strips,

wander in relative phase, and increase by a factor of 1.7 between cycle 10 and cycle 161,120, and a factor 4.8 between cycle 10 and cycle 249,650. These changes are not proportional because monotonically increasing material damage does not necessarily entail additive increments of magnetization.

6. Discussion and Summary

The feasibility of correlating magnetization changes with the progression of fatigue in steel was first demonstrated by H. Weinstock and collaborators [58-63]. Since several of these tests used 1018 steel samples from the same source that supplied material for the present series of measurements a direct comparison of the results is possible. In particular, Figs. 3-5 of reference [58] and Fig. 4 of reference [59] indicate field variations of the order of 200 nT or 2 mG associated with stress cycles in the range 40-275 MPa or 6-40 ksi. Allowing for the fact that these magnetic fields were detected by SQUID gradiometers whose sensing elements were separated from the samples by effective distances of at least 2.2 cm [41,59,62], these results are quantitatively consistent with the present measurements. Similar magnetic field values were obtained with cold-worked and annealed specimens of E24-2 (French) steel [59,60]. There are several other common features shared by these experiments: (*i*) The hysteresis loops depicted in Fig. 1(c) of reference [60] resemble the piezomagnetic ducks in Fig. 6(b); and (*ii*) after prolonged cycling, the hysteresis loops in [59] and [62] tend to enlarge, paralleling the field increases

that appear in the last strip chart in Fig.16. (*iii*) The classic Villari reversals also appear in many field traces such Fig.1 and Figs. 4(a)-5(c) in [58], Fig. 3 in [59], and form the apex of all the ducks' heads in Fig. 6(b). This non-monotonic relation between magnetization and stress is usually explained as the combined effect of domain wall movements and domain rotations: Or, in quantitative terms, by a competition between magnetocrystalline energy (~K) and magnetoelastic energy (~ $\lambda\,\sigma$) where λ is the magnetostrictive constant and σ is stress [4,5]. But the simplest versions of these models are clearly inadequate. For instance, in iron $K \sim 4 \times 10^5$ ergs/cm^3 and $\lambda \sim 10^{-5}$. Therefore, even at higher stress levels, such as $\sigma \sim 330$ MPa or 50 ksi, these crude estimates would indicate that magnetoelastic effects are comparatively small. However, most of the piezomagnetic measurements reflect complex and sensitive interactions between stress and magnetization --- some of the data exhibits field reversals for stresses as low as 38 MPa or 5.5 ksi. In addition, all the simple domain models ignore the progressive changes wrought by fatigue. Consequently there is as yet no explanation of the fact that all the field reversals encountered during increasing strain cycles in Fig. 6(b) have disappeared from the 'old' duck profiles in Fig. 8(b).

With all this information at hand, it is likely that doubts about the observability of piezomagnetic effects will finally disappear from the literature [64, 65], and future

research will concentrate on refining the connections between piezomagnetism and fatigue There are at least five principal problems areas:

(1) Both experimental results and theoretical estimates show that when 1018 steel is subjected to cyclic loading with peak stresses comparable to the yield strength (~ 70 ksi or 480 MPa), the damage per cycle is equivalent to the generation of the order of 10^{17} defects/cm^3, and these mesoscopic transformations are sufficiently extensive to produce measurable changes in magnetization (~ 10^{-3} emu or 10^{-6} Am^2) that distinguish every cycle. Clearly, under these conditions piezomagnetic effects are as large as they can be --- short of outright fracture --- and the basic *inverse problem* is to relate the observed field profiles, such as those in Figs. 6(a) - 6(b), and the 'infarct' at cycle 4363 in Figs. 14 and 15, to various mesoscopic damage mechanisms. The usual method of dealing with such situations is to model the direct problem with a simple set of standard sources --- multipoles in static field problems, and a suitable set of artificially constructed defects in the piezomagnetic case. Practical examples would include composite specimens containing voids and cracks of known dimension and orientation, with or without prior surface magnetization.

(2). The basic fatigue problem, illustrated in Fig. 1, is to predict the total number of cycles to failure N_f for a particular specimen and a predetermined loading program at the earliest

possible moment. Extensive tests with 1018 steel specimens have shown that a practical route to a solution is to devise quantitative measures of the changes that occur in the properties of the stress-strain hysteresis loops as the number of cycles N increases. Two indices of this kind are shown in Fig. 1 : the variation of the hysteresis loop areas, or energy dissipation per volume $\Delta U(N)$; and the hysteresis loop distances $D\{\mathcal{L}(1); \mathcal{L}(N)\}$, which measure the change in shape and position of the stress-strain loci between cycles 1 and N. The crucial experimental observation is that although the specific values of the N_2 transition in Fig. 1 may fluctuate widely from run to run, the ratio $N_2/N_f \simeq 12$ % tends to be stable [44-46]. In this sense, purely mechanical measurements can indeed lead to reliable 'early warnings' of eventual fatigue failure.

The basic question now is whether the additional information furnished by piezomagnetic effects can improve the accuracy and reliability of the mechanical failure predictions. A favorable augury is the much greater sensitivity of magnetic response in comparison to mechanical diagnostics --- the magnetic detection of the 'silent infarct' in the lower strip of Fig. 14 is a striking example. But in the absence of any detailed theories relating piezomagnetism to fatigue it is not certain that the cumulation of mesoscopic damage can be correlated with any monotonically varying indices of magnetization that yield well-defined markers such as the N_2 transition. Again, there are some favorable

indications: Under repeated stress, non-magnetic 304 stainless steel can partially convert from the austenitic to the ferromagnetic martensitic phase, and this proportional transformation can be detected with the help of auxiliary bias fields and suitable sensors [9,10,66]. There also appears to be a gradual enlargement of the piezomagnetic loops as the samples age, but this trend requires further quantitative confirmation. Perhaps the most promising approach is to recast the hysteresis loop distances in a form suitable for providing a quantitative measure of the three - dimensional deformations that are so prominent in Fig. 5. Since stress σ and field (squared) B^2 are both dimensionally equivalent to energy densities, an obvious generalization of the expression in [46] is

$$D \sim \sum_{K} \{ \mid \sigma (\epsilon_K , N_i) - \sigma (\epsilon_K , N_j) \mid + \gamma [B (\epsilon_K, N_i) - B (\epsilon_K, N_j)]^2 \}. \qquad (6.1)$$

Formally this yields a distance between the i^{th} and j^{th} loops: γ is a dimensionless constant that allows for some adjustment to fit the scale of the measurements. Other metric choices can also be adapted to measure hysteresis 'distances' [67]. Figure 17 shows the initial results of this type of analysis applied to the deformations of the ducks' heads in Fig. 6(a) and Fig. 8(a). It is straightforward to quantify the progressive narrowing of the $B - \epsilon$ traces in the interval $0 \leq \epsilon \leq 0.008$ by averaging the field differences on the ascending

and descending branches of the hysteresis loops. A comparison with Fig. 7 shows the contrasting behavior: a steady evolution of the magnetic traces in Fig. 17, while the corresponding mechanical index $\Delta U(N)$ hardly varies in the interval $25 < N < 325$.

(3). In may practical situations the important unknown is the remaining service life $N_f - N$ and not the total life N_f. Since in these cases neither the elapsed time, i.e. N, nor the no--minal life expectancy N_f may be available from separate measurements, the problem of predicting fatigue failure is compounded. It is especially difficult in high cycle fatigue where the probability that random inspections happen to fall either into the initial accommodation stage $N < N_2$ or occur during terminal failure $N > N_3$ is less than 20%. The essential problem --- as is apparent from Fig. 1 --- is that in these cases fatigue measurements are made somewhere during the long accretion of damage stage where all the variables --- magnetic as well as mechanical --- change imperceptibly from cycle to cycle. One general approach to gauging the intrinsic age or level of accumulated damage in a specimen during this stage is to superpose some external load or 'injury' during one or more cycles, and then to measure the rate of recovery as the normal loading cycles are resumed. This method has been tried with mechanical hysteresis measurements, but the observed rates of recovery from overloads are not sufficiently sensitive to detect the intrinsic levels of damage. It remains to be seen whether the enhanced sensitivity of magnetic measurements will lead to useful results [61].

(4). It is well known that steel has a fatigue or endurance limit, that is, a loading level be-

low which specimens can sustain a very large number of cycles ($N > 10^7$) without exhibiting any tendency towards eventual fatigue failure [68]. Because of their obvious technical importance, values of the fatigue limit for various alloys are tabulated in many standard handbooks such as [69], and are the object of ongoing testing programs in industrial research organizations. There are two practical difficulties that hamper these measurements: (1) The standard 'S - N' tests are time consuming because the trials usually have to be prolonged until the number of cycles reaches $N > 10^6$; and (2) there is an inherent statistical scatter in the results which is reminiscent of the dispersion in fatigue life measurements [43]. Since the piezomagnetic Villari reversals are associated with the inception of plastic flow, it has been suggested that magnetic measurements could provide a speedier means for determining the endurance limit of individual specimens [58]. Certainly it has been demonstrated that in ferromagnetic materials piezomagnetic measurements yield more detailed information concerning mesostructural rearrangements than purely mechanical measurements. But it is not clear that a simple field reversal is an adequate signature of the endurance limit.

The existence of a stable value for the ratio N_2/N_f for many 1018 steel specimens indicates a causal connection between the end of the accommodation stage in Fig. 1 and

the number of additional cycles required to reach final failure. This relation may be interpreted as a dynamic version of French's concept of a critical damage curve [70]. The essential assumption is that the N_2 transition represents the *maximum* possible accommodation of the material's mesostructure to the imposed loading conditions. If this accommodation is imperfect in the sense that with every succeeding cycle, $N > N_2$, additional damage is generated then obviously there must be eventual failure. On the other hand, if the accommodation is complete, then further loading cycles may generate non-vanishing hysteresis loops; but these loops would simply correspond to the conversion of mechanical work into heat without any concomitant damage. Clearly this represents a shift in emphasis --- the endurance limit is identified with the asymptotic behavior of an accommodation process rather than merely a critical load level. Since cyclic loading at or below the endurance limit is in principle equivalent to infinite life, practical tests involve long time scales for all the fiducial markers including the N_2 transition. Nevertheless, because the exponential rate of approach to maximum accommodation is associated with the shortest time scale of all the relevant processes (except for final fracture) there is a possibility that piezomagnetic measurements may accelerate the determination of N_2, and thereby sharpen estimates of the endurance limit.

(5) The SQUID magnetometer measurements described in [58-60,62,63] were all acquired using the least sensitive scales of the instruments. Accordingly, there is no doubt

that piezomagnetic field variations can be detected in materials such as aluminum alloys that contain only small proportions of ferromagnetic components. Magnetometers with increased sensitivity and greater bandwidth will also make it possible to detect the Barkhausen pulses that accompany mechanical stress. As indicated in sub-section 4 of the introduction, the Kaiser effect is a pervasive regularity both of acoustic and Barkhausen emission that is associated with reversible behavior below the endurance limit [39-41,52]. Recent published and unpublished results show that even after the transition to irreversible behavior, due to larger field sweeps or strain excursions, both the magnetic as well as the mechanical 'noise' signals contain a sub-population of stable patterns that recur in a semi-regular fashion from cycle to cycle [71,72]. It is plausible to link these regularities with localized mesoscopic 'toggles' whose switching sequences are actuated by macroscopic hysteresis. Presumably, during fatigue the characteristics of these patterns will change, and may occasionally 'spike up', until there is an avalanche culminating in a giant event such as the 'infarct' in cycle 4363 of Fig. 15.

Acknowledgments

We would like to thank Dr. H. Weinstock for many informative discussions as well for furnishing unpublished data.

This work was supported by the grants from the US Air Force Office of Scientific Research.

References

[1] Joule JP 1847 Phil. Mag. ser.3, 30, 76-87, 225-241; The Scientific Papers of J.P. Joule, vol.I, 235-264 (London: Dawsons of Pall Mall, 1963)

[2] Reed IM, Greenough RD and Jenner AGI 1995 IEEE Trans. Magn. 31, No.6, 4038-4040

[3] Nagaoka H 1894 Ann. Physik 53, 487-498

[4] Becker R and Doring W 1939 Ferromagnetismus (Berlin: Springer Verlag)

[5] Bozorth RM 1951 Ferromagnetism (Princeton: van Nostrand)

[6] Kneller E 1962 Ferromagnetismus (Berlin: Springer Verlag)

[7] Gilbert W 1600 De Magnete (London: P.Short); 1958 (New York: Dover)

[8] Villari E 1865 Ann. Physik 126, 87-122

[9] Thompson LD and Westermo B 1992 Advance in Instrumentation and Control 47, part 2, 1295-1303

[10] Westermo B (private communication, 1996)

[11] Bozorth RM and Williams HJ 1945 Rev. Mod. Phys. 17, 72-80

[12] Atherton DL and Jiles DC 1983 IEEE Trans. Magnetics MAG-19, No.5, 2021-2023

[13] Langman R 1985 IEEE Trans. Magnetics MAG-21, No.4, 1314-1320

[14] Kwun H and Burkhardt GL 1987 J. Appl. Phys. 61, No.4, 1576-1579

[15] Sablik MJ, Kwun H, Burkhardt GL and Jiles DC 1987 J. Appl. Phys. 61, No.8, 3799-3801

[16] Sablik MJ, Burkhardt GL, Kwun H and Jiles DC 1988 J. Appl. Phys.63, No.8, 3930-3932

[17] Sablik MJ, Rubin SW, Riley LA, Jiles DC, Kaminski DA and Biner SB 1993 J. Appl. Phys. 74, No.1, 480-488

[18] Makar JM and Atherton DL 1994 IEEE Trans. Magnetics 30, No.4, 1380-1387

[19] Makar JM and Atherton DL 1995 IEEE Trans Magnetics 31,No.3, 2220-2227

[20] Puppin E and Callegaro L 1996 IEEE Trans Magnetics 32, No.1, 281-284

[21] Jiles DC 1988 NDT International 21, No.5, 311-319

[22] Jiles DC 1990 NDT International 23, No.2, 83-92

[23] Jiles DC 1995 J.Phys. D: Appl. Phys. 28, 1537-1546

[24] Portevin A and Le Chatelier MA 1923 Comptes Rend Acad Sci 176, 507-510

[25] Hall EO 1970 Yield Point Phenomena in Metals and Alloys (New York: Plenum)

[26] Bell JF 1968 The Physics of Large Deformation of Crystalline Solids (New York: Springer)

[27] Erber T, McGreer KA, Nowak ER, Wan JC and Weinstock H 1990 J. Appl. Phys.68,1370-1372

[28] Kaiser J 1950 Untersuchungen uber das Auftreten von Gerauschen beim Zugversuch Dr.Ing.Diss.Techn.Hochsch.Munchen

[29] Barkhausen H 1919 Phys Zeit. 20, 401-403

[30] Heaps CW and Bryan AB 1930 Phys. Rev.36, 326-332

[31] McClure JC, Bhattacharya S and Schroder K 1974 IEEE Trans. Magnetics MAG-10, No.3, 913-915

[32] Tiitto K 1987 'Use of Barkhausen Effect in Testing for Residual Stresses and Material Defects' Conf. on Residual Stress in Design, Process and Material Selection, Cincinnati, Ohio

[33] Tiitto K 1989 Nondestr. Test. Eval. 5, 27-37

[34] American Stress Technologies, Pittsburg PA 1990 'Magnetoelastic Instrumentation- Rollscan'

[35] Ogden WP 1991 'Detection of Subsurface Tensile Stress in an Aircraft Engine Mainshaft Bearing Using Barkhausen Noise' ASM Conf. on Practical Applications of Residual Stress Technology, Indianapolis, Indiana

[36] Barkhoudarian S 1996 NASA Tech Briefs 20, No.8, 48

[37] Jiles DC, Kern R and Theiner WA 1993 Nondestr. Test. Eval. 10, 317-331

[38] Jiles DC and Suominen L 1994 IEEE Trans. Magnetics 30, No.6, 4924-4926

[39] Pasztor G and Schmidt C 1978 J. Appl. Phys. 49, 886-899

[40] Erber T, Porteseil JL and Molho P 1985 Phil. Mag. B52, 963-969

[41] Weinstock H, Erber T and Nisenoff M 1985 Phys. Rev.B31, 1535-1553

[42] Bernstein B, Karamolengos M and Erber T 1993 Chaos, Solitons & Fractals 3, N No.3, 269-277

[43] Sobczyk K and Spencer Jr. BF 1992 Random Fatigue: From Data to Theory (Boston: Academic Press)

[44] Erber T, Guralnick SA and Michels SC 1993 Annals Phys (NY) 224, No.2, 157-192

[45] Erber T, Guralnick SA and Desai RD 1994 Proc. 12th Natl. Congr. Appl. Mech. 185

[46] Erber T and Guralnick SA 1994 Am. Math.Soc. Abstr.15, No.6, 574

[47] Zhang Y and Atherton DL 1995 IEEE Trans. Magnetics 31, No.3,2233-2239

[48] Dessler AJ, Michel FC, Rorschach HE and Trammell GT 1968 Phys. Rev.168, 737-743

[49] Herring C 1968 Phys. Rev.171, 1361-1369

[50] Maris HJ 1974 Phys. Rev. Lett. 33, No.19, 1177-1180

[51] Guralnick SA, Singh S and Erber T 1984, ASCE, J.Structural Engin.110, No.9, 2103-2119

[52] Erber T and Guralnick SA 1988 Annals Phys (NY) 181, No.1, 25-53

[53] Bever MB, Holt DL and Titchener AL 1973 Progr. Materials Sci 17, 1-177

[54] Puskar A and Golovin SA 1985 Fatigue in Materials: Cumulative Damage Processes (New York: Elsevier)

[55] Nuti JE, Erber T and Guralnick SA 1976 Phys Lett 57A, No.4, 357-358

[56] Nuti JE 1977 M.Sc. Dissertation, IIT, Chicago

[57] Erber T, Marousek GR and Forsberg GK 1969 Acta Phys. Austriaca 30, 271-294

[58] Mignogna RB, Browning V, Gubser DU, Schechter RS, Simmonds KE and Weinstock H 1993 IEEE Trans. Appl. Supercond. 3, No.1, pt. 4, 1922-1925

[59] Banchet J, Jouglar J, Vuillermoz P.-L., Waltz P and Weinstock H 1995 Rev. of Progr. in Quantitative Nondestructive Eval. Eds. D.O. Thompson & D. E Chimenti, vol. 14b, 1675 - 1682

[60] Banchet J, Jouglar J, Vuillermoz P.-L., Waltz P and Weinstock H 1995 IEEE Trans. Appl. Supercond. 5 No. 2, pt. 3, 2486 - 2489

[61] Weinstock H 1995 US Patent 5,423,223

[62] Banchet J and Waltz P 1994 'Le SQUID Applique a l'Etude des Domaines Ferromagnetiques' Institut National des Science Appliquees, Lyon

[63] Melquiond F, Mouroux A, Jouglard J, Vuillermoz P.-L. and Weinstock H 1996 J.Magn. Magnetic Mat. 157/158, 571-572

[64] Voigt W 1928 Lehrbuch der Kristallphysik (Leipzig: Teubner)

[65] Misra A and Varshney BG 1990 J. Mag. and Magnetic Mat. 89, 159-166

[66] Otaka M, Enomoto K, Hayashi M, Sakata S and Shimizu S 1994 ASME, Pressure Vessels and Piping 276, 113-117

[67] Erber T, Schweizer B and Sklar A 1971 Commun. Math. Phys. 20, 205-219

[68] Cyclic Deformation and Fatigue of Metals 1993 Ed. M. Bily (Amsterdam: Elsevier)

[69] Baumel Jr. A and Seeger T 1990 Materials Data for Cyclic Loading, Suppl. 1 (Amsterdam: Elsevier)

[70] French HJ 1933 Trans. Am. Soc. Steel Treating 21, 899-945

[71] Petta JR, Weissman MB and O'Brien KP 1996 Phys. Rev. E54, 1029-1031

[72] R. Zasadzinski 1997, private communication

Figure Captions

Figure 1. The principal stages of fatigue. The diagram shows the evolution of two damage indices---hysteresis loop areas and distances [44]---derived from stress-strain measurements of a 1018 steel specimen. In this case the strain range was 0.0018, and fatigue failure occurred at 1489 cycles. The significance of the transition points at N_2 and N_3 is discussed in the text. The ordinate scales are in engineering units of energy density; 1 kip-in/in^3 = 6.895 J/cm^3, where 'kip' denotes a thousand pounds.

Figure 2. Schematic of the measuring equipment. The fatigue specimens---shown in the inset---are subjected to cyclic loading by an MTS-810 servohydraulic test machine. Stress, strain, magnetic and acoustic data for every loading cycle can be processed by an array of computers.

Figure 3. Magnetomechanical response of a steel specimen during a single loading cycle. The central box displays the resulting hysteresis in a three-dimensional space spanned by stress, strain and magnetic field. The top panel shows that the usual stress-strain hysteresis loops are merely one projection of a much more intricate three-dimensional locus.

Figure 4(a) and 4(b).

These are rotated and enlarged views of the magnetomechanical hysteresis locus in the central box of Fig. 3. The open circles represent data points recorded during the strain controlled cycling of a 1018 steel specimen with $\epsilon \leq 0.018$ and a stress range $-60 \text{ ksi} \leq \sigma \leq +72 \text{ ksi}$. (1 ksi = 10^3 lbs/in^2 = 6.895 MPa.) The magnetic field scales are in Volts, where 1 V is equivalent to 41.6 mG at the fluxgate sensor. The upper trace shows the data for cycle 10, the lower trace for cycle 340.

Figure 5. Overlay of the the two traces in Fig. 4(a) and 4(b): the solid curve corresponds to cycle 10 and the dashed curve to cycle 340. The prominent changes in shape and position of the piezomagnetic response are due to the cumulative effects of fatigue.

Figure 6(a). Eight consecutive strain-field hysteresis cycles. Cycle 10 is the front projection of the trace in Fig. 4(a). In virtue of the large damage generated during each of these loading cycles, every hysteresis locus in this sequence has a different shape.

Figure 6(b). Eight consecutive stress-field hysteresis cycles. Cycle 10 is a side projection of the trace in Fig. 4(a).

Figure 6(c). Eight consecutive stress-strain hysteresis cycles. Cycle 10 is a top projection of the trace in Fig. 4(a). The dashed lines in cycle 9 show the strain values corresponding to the transitions between tension and compression. In contrast to the piezomagnetic traces, all of these loops have very nearly the same shape.

Figure 7. Plot of the hysteresis loop area as a function of the number of loading cycles. The data corresponds to the experiment of Figure 4(a) and 4(b). The shape of this curve closely resembles the dashed curve in Fig. 1.

Figure 8(a). Eight consecutive strain-field hysteresis cycles. Cycles 340 is the front projection of the trace in Fig. 4(b); the two vertical arrows indicate a feature discussed in the text.

Figure 8(b). Eight consecutive stress-field hysteresis cycles. Cycles 340 is a side projection of the trace in Fig. 4(b).

Figure 9. Overlay of hysteresis curves from cycle 10 (solid lines) and cycle 340 (dashed lines) showing the effects of fatigue. These panels are the three orthogonal projections of Fig. 5. It is obvious that the minimum variations are exhibited by the conventional stress-strain hysteresis loops.

Figure 10. Hysteresis loop sequences illustrating the rapid pace of deformations that occurs during terminal failure.

Figure 11. Strain, magnetic field and stress plotted as functions of time. These traces are fold-outs of some of the data in Figs. 6(a) - 6(c). This format emphasizes the correlations between the magnetic field variations and the peak strain reversals [SR], zero strain reversals [SR(O)], zero stress transitions [O], and the proportional limit [P]. The D-arrows correspond to the double point in the duck tail of cycle 10 in Fig. 6(a).

Figure 12. Strain, magnetic field and stress plotted as functions of time. These traces show the continuation of the measurements in Fig. 11 during the late stages of fatigue in a sample that failed at about 368 cycles.

Figure 13. Overlay of cycles 11,12, from Fig.11 (solid lines) and cycles 301, 302 from Fig. 12 (dashed lines). The magnetic field trace intersections at the O and P points indicate positions of minimal variation during the progressions of fatigue. The largest changes occur in the vicinity of zero stress SR(O) and maximum compression, of Fig. 9.

Figure 14. Strain, magnetic field and stress plotted as functions of the time for a fatigue experiment where failure occurred at 4716 cycles. The difference between the early and late magnetic traces show the cumulative effects of fatigue. An 'infarct', probably due to a microfracture, is visible in cycle 4363. The calibration for the magnetic ordinate scales is $0.1\text{V} \cong 14$ mG.

Figure 15. Enlarged view of the magnetic field sequence of Fig. 14 including the large excursion at cycle 4363. The prominent cleft at point C is apparently a precursor. Although the shapes of the magnetic peaks are quite different on either side of cycle 4363, the valley contours between the pairs of F-arrows are indistinguishable.

Figure 16. Strain profile and magnetic field traces from a high cycle fatigue experiment where failure occurred at 250, 245 cycles. The calibration of the ordinate scale is approximately the same as in Fig. 14 and Fig. 15: $0.1\text{V} \simeq 14$ mG. At these lower strain levels ($\epsilon \leq 0.0035$) the field maxima M nearly coincide with the strain minima. Evidently, there is a large field increase just before final failure.

Figure 17. A quantitative measure of piezomagnetic hysteresis loop deformations. Figures 6(a) and 8(a) show marked changes in the shapes of the ducks' head for strain ranges $0 \leq \epsilon \leq 0.008$. This graph is a simple numerical approximation of the average spacing between the magnetic traces in this interval.

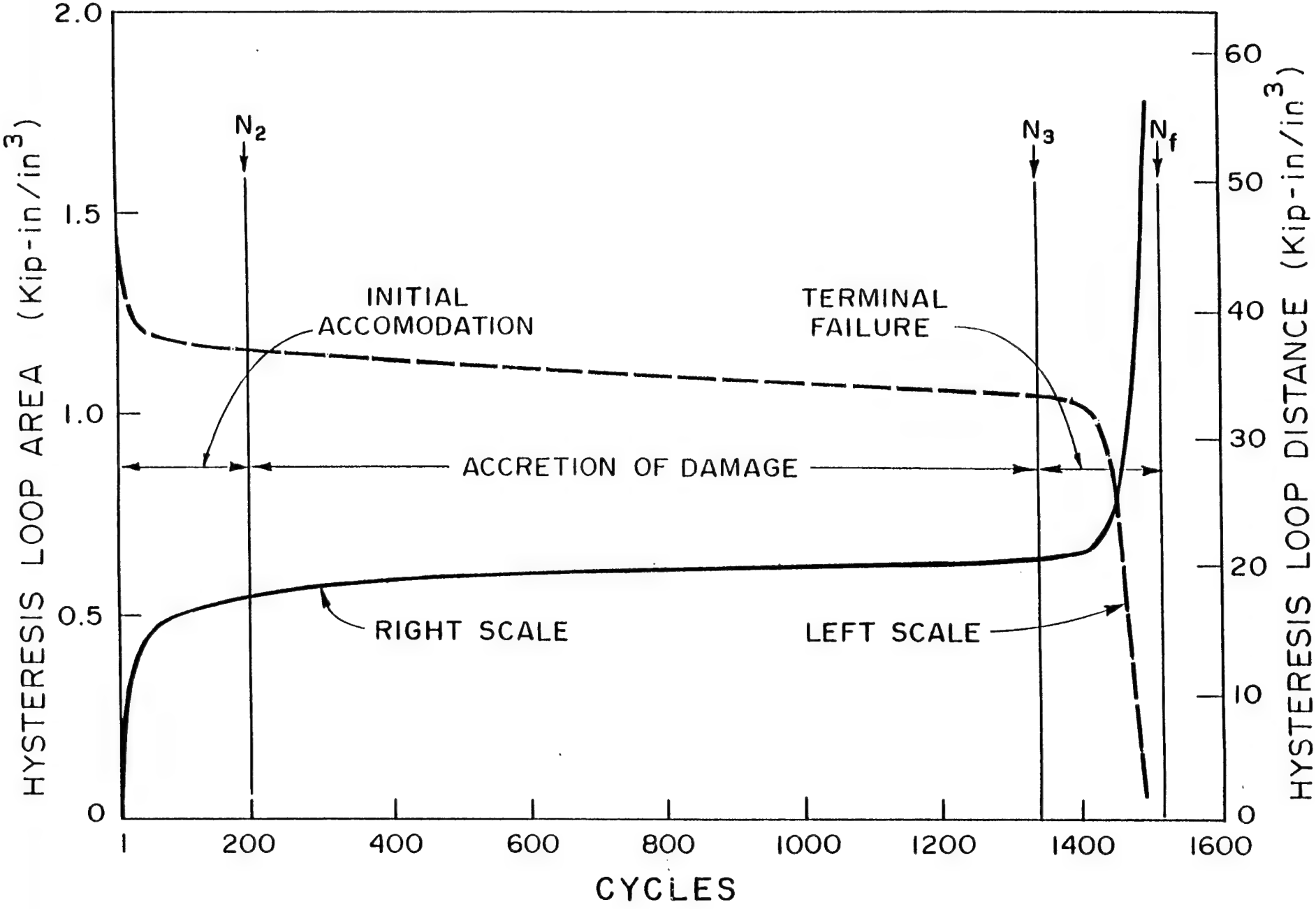
2.0
1.5
1.0
0.5
0
HYSTERESIS LOOP AREA (Kip-in/in^3)
60
50
40
30
20
10
0
HYSTERESIS LOOP DISTANCE (Kip-in/in^3)
N_2
N_3
N_f
INITIAL ACCOMODATION
TERMINAL FAILURE
ACCRETION OF DAMAGE
RIGHT SCALE
LEFT SCALE
1
200
400
600
800
1000
1200
1400
1600
CYCLES

Fig. 1

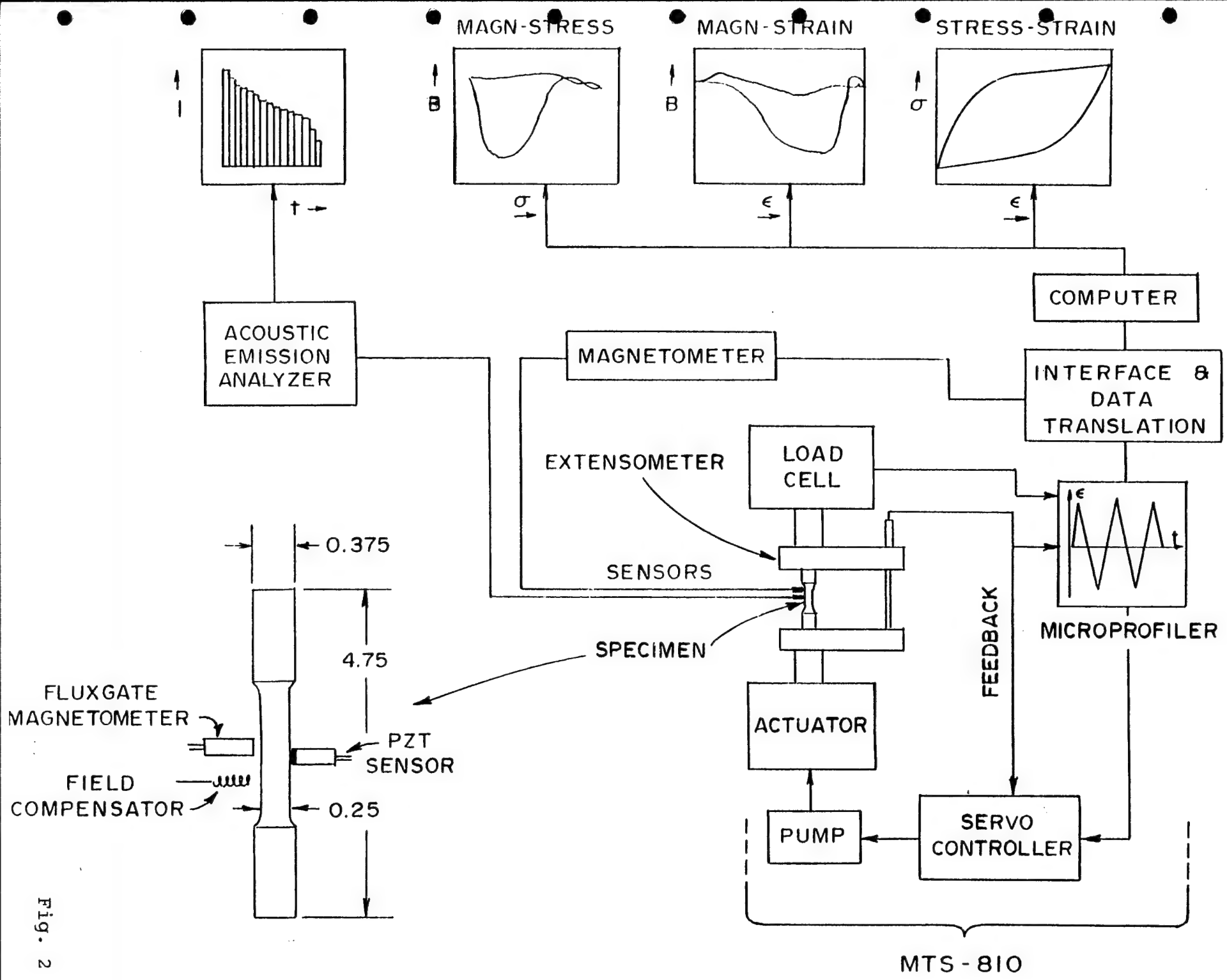
MAGN-STRESS
MAGN-STRAIN
STRESS-STRAIN
I
t
B
σ
B
ϵ
σ
ϵ
COMPUTER
ACOUSTIC EMISSION ANALYZER
MAGNETOMETER
INTERFACE & DATA TRANSLATION
EXTENSOMETER
LOAD CELL
SENSORS
SPECIMEN
FEEDBACK
MICROPROFILER
ϵ
t
0.375
4.75
FLUXGATE MAGNETOMETER
PZT SENSOR
FIELD COMPENSATOR
0.25
ACTUATOR
PUMP
SERVO CONTROLLER
MTS-810

Fig. 2

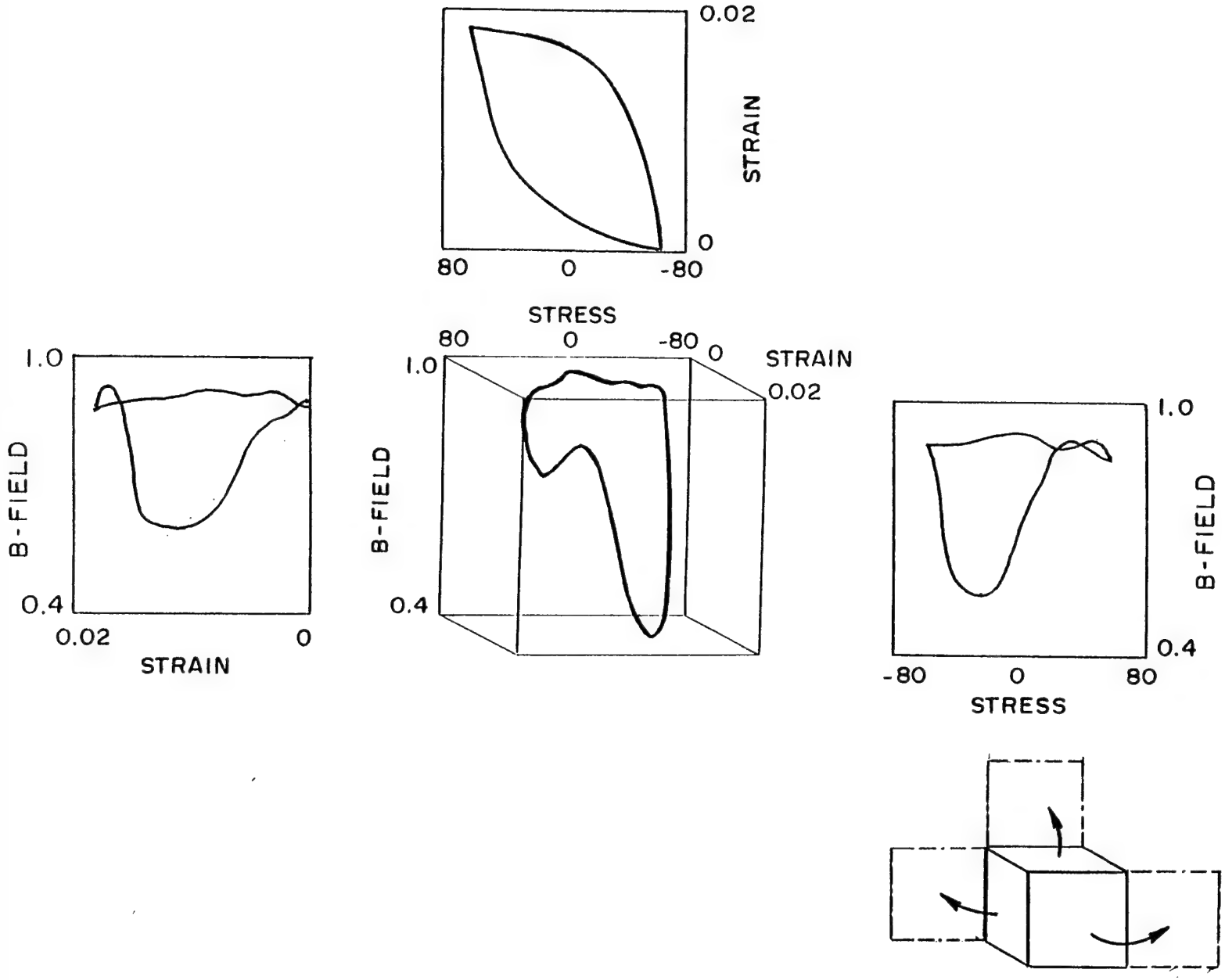
0.02
STRAIN
0
80
0
-80
STRESS
1.0
B-FIELD
0.4
0.02
0
STRAIN
80
0
-80
0
STRAIN
1.0
B-FIELD
0.02
0.4
1.0
B-FIELD
0.4
-80
0
80
STRESS

Fig. 3

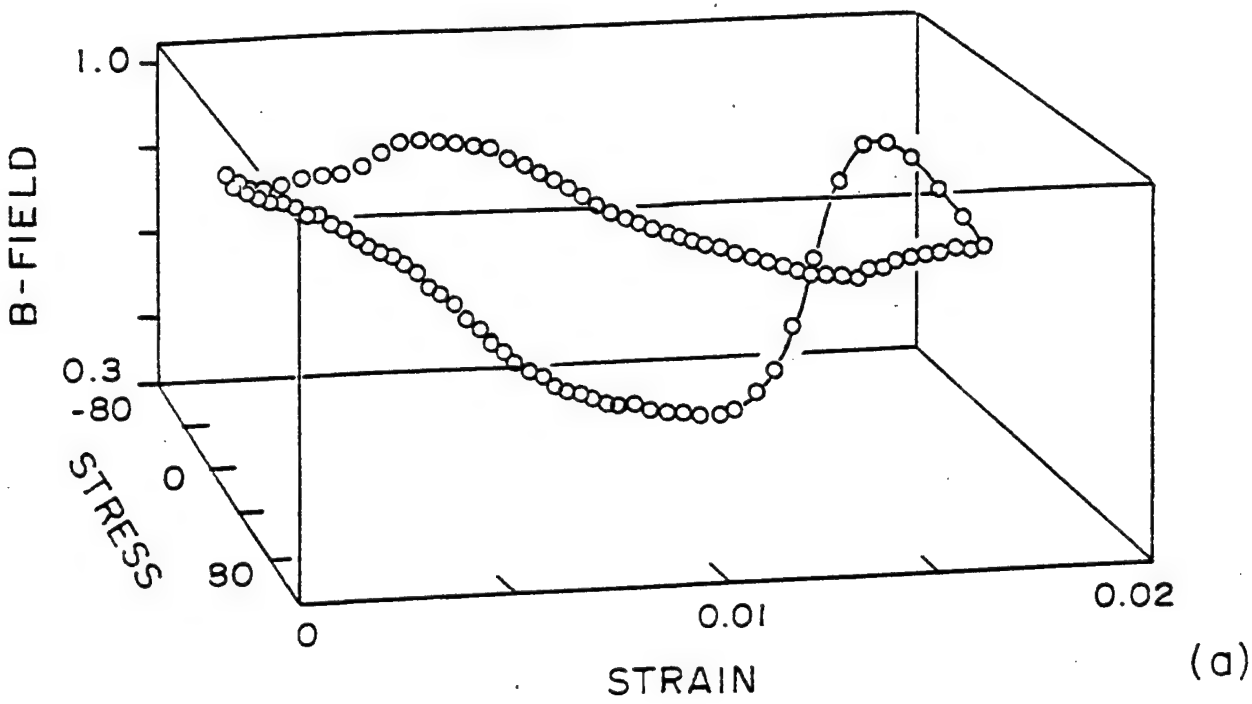
1.0
B-FIELD
0.3
-80
STRESS
0
80
0
0.01
0.02
STRAIN

(a)

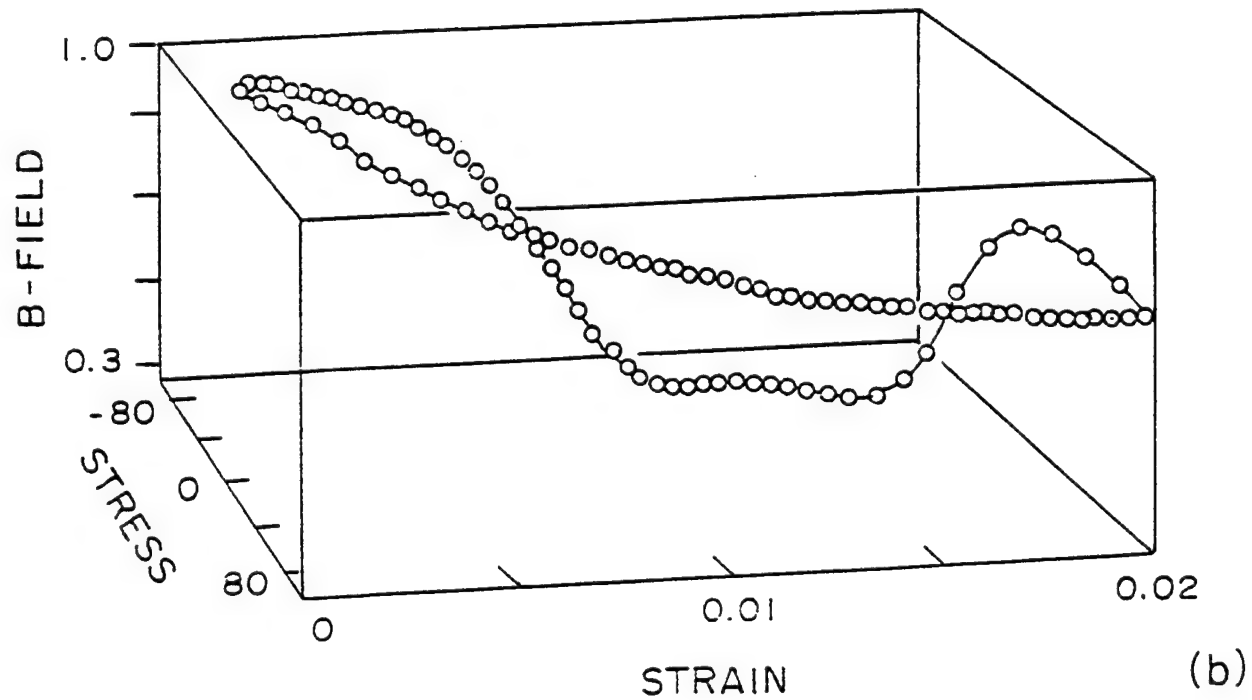
1.0
B-FIELD
0.3
-80
STRESS
0
80
0
0.01
0.02
STRAIN

(b)

Fig. 4

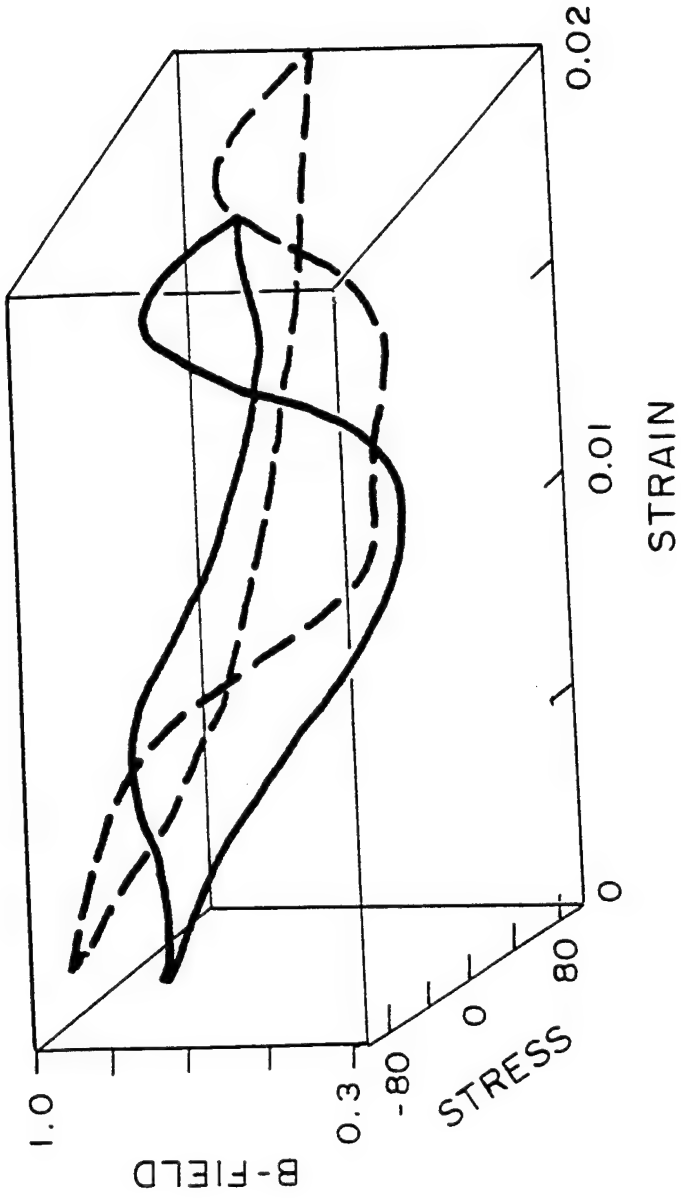

Fig. 5

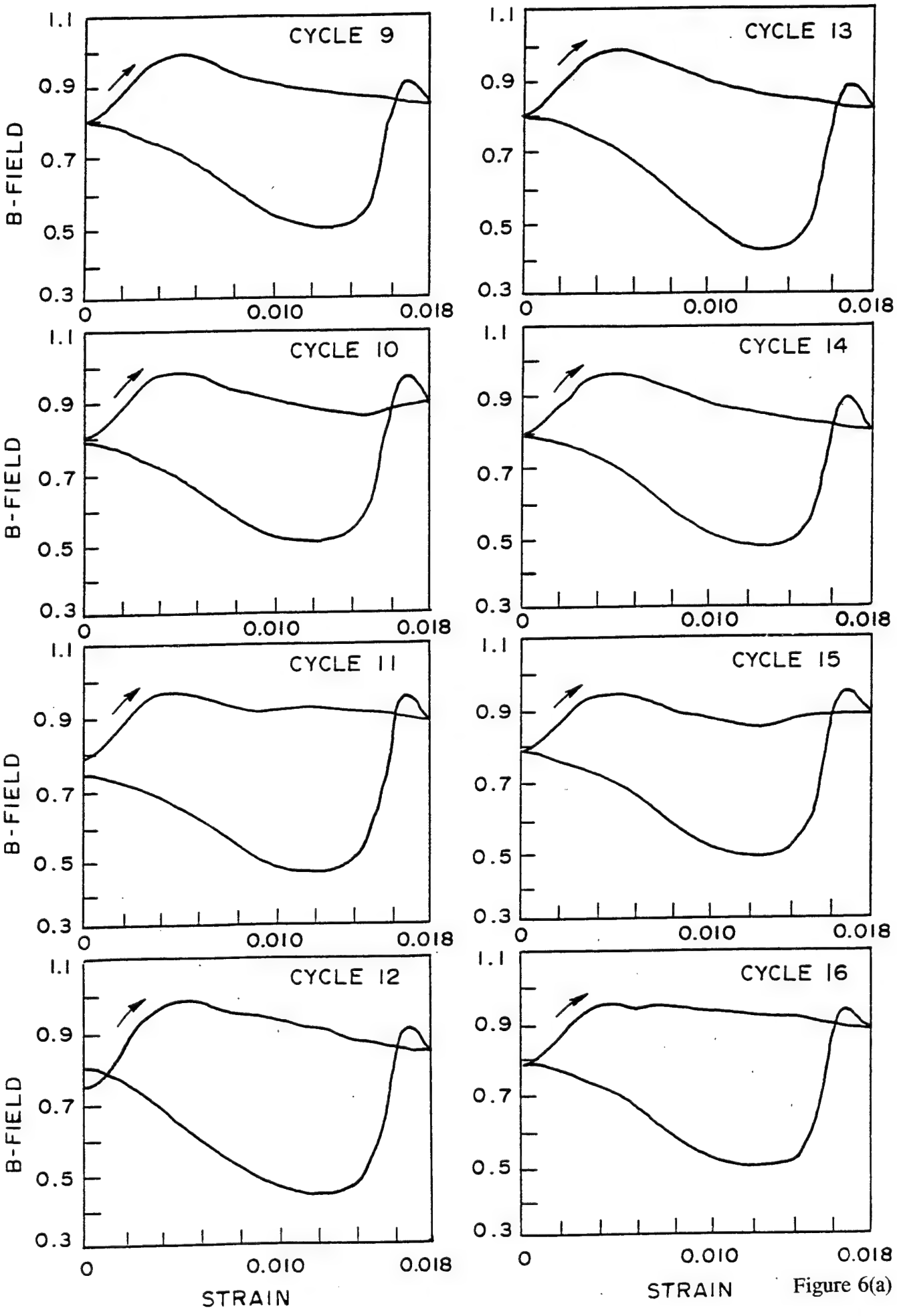
CYCLE 9
CYCLE 13
CYCLE 10
CYCLE 14
CYCLE 11
CYCLE 15
CYCLE 12
CYCLE 16
B-FIELD
STRAIN
1.1
0.9
0.7
0.5
0.3
0
0.010
0.018

Figure 6(a)

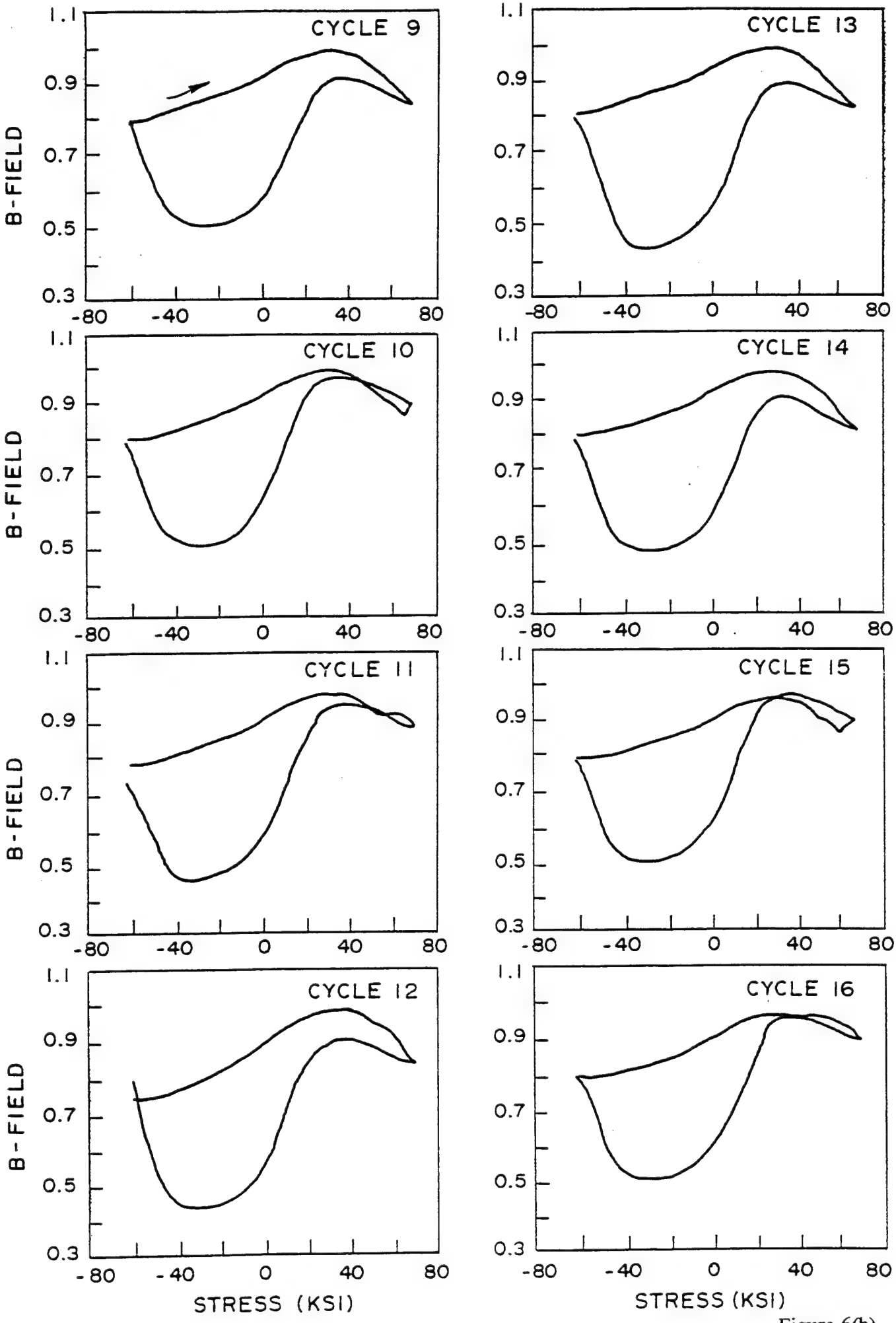
CYCLE 9
CYCLE 13
CYCLE 10
CYCLE 14
CYCLE 11
CYCLE 15
CYCLE 12
CYCLE 16
B-FIELD
1.1
0.9
0.7
0.5
0.3
-80
-40
0
40
80
STRESS (KSI)

Figure 6(b)

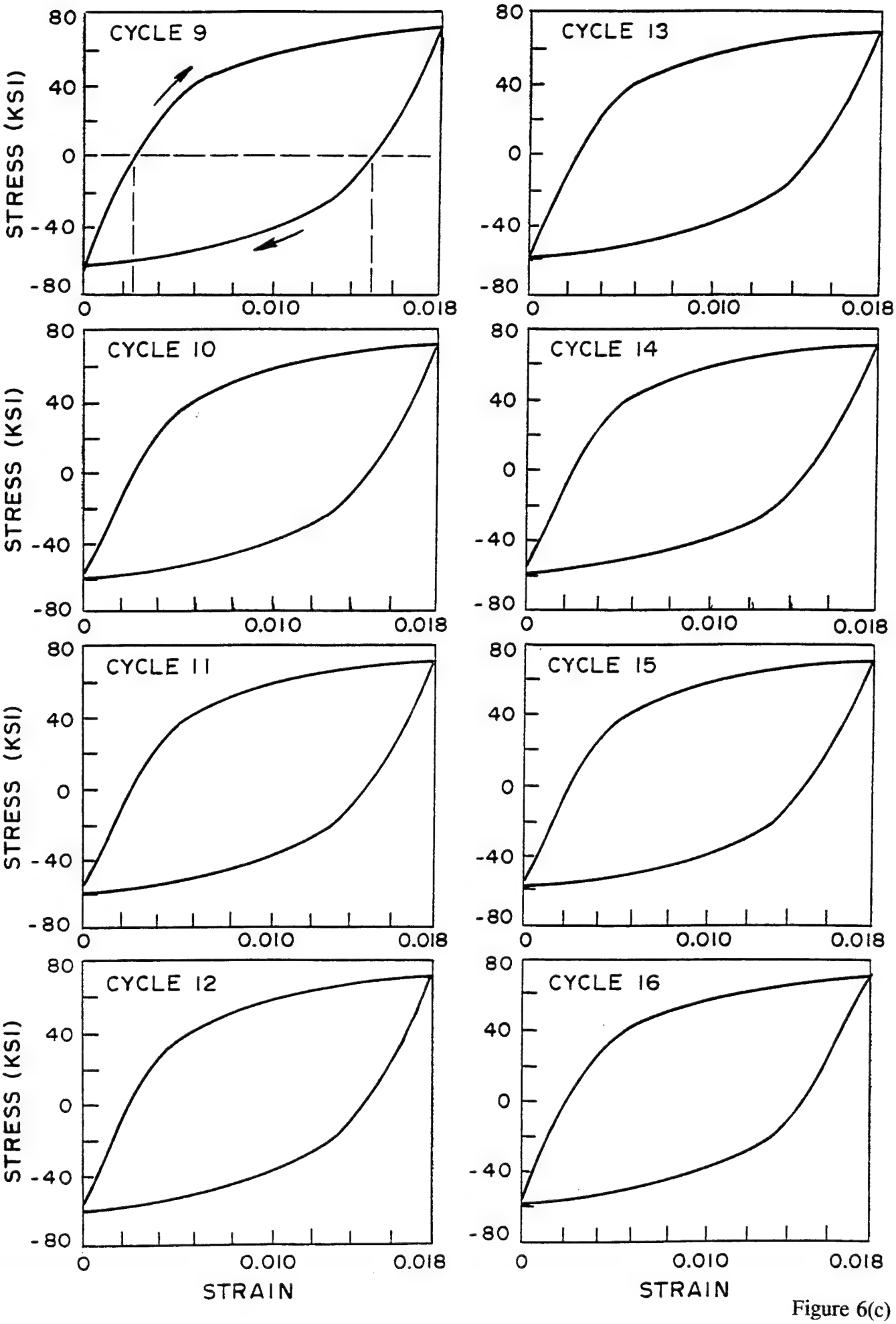
CYCLE 9
CYCLE 10
CYCLE 11
CYCLE 12
CYCLE 13
CYCLE 14
CYCLE 15
CYCLE 16
STRESS (KSI)
STRAIN
80
40
0
-40
-80
0
0.010
0.018

Figure 6(c)

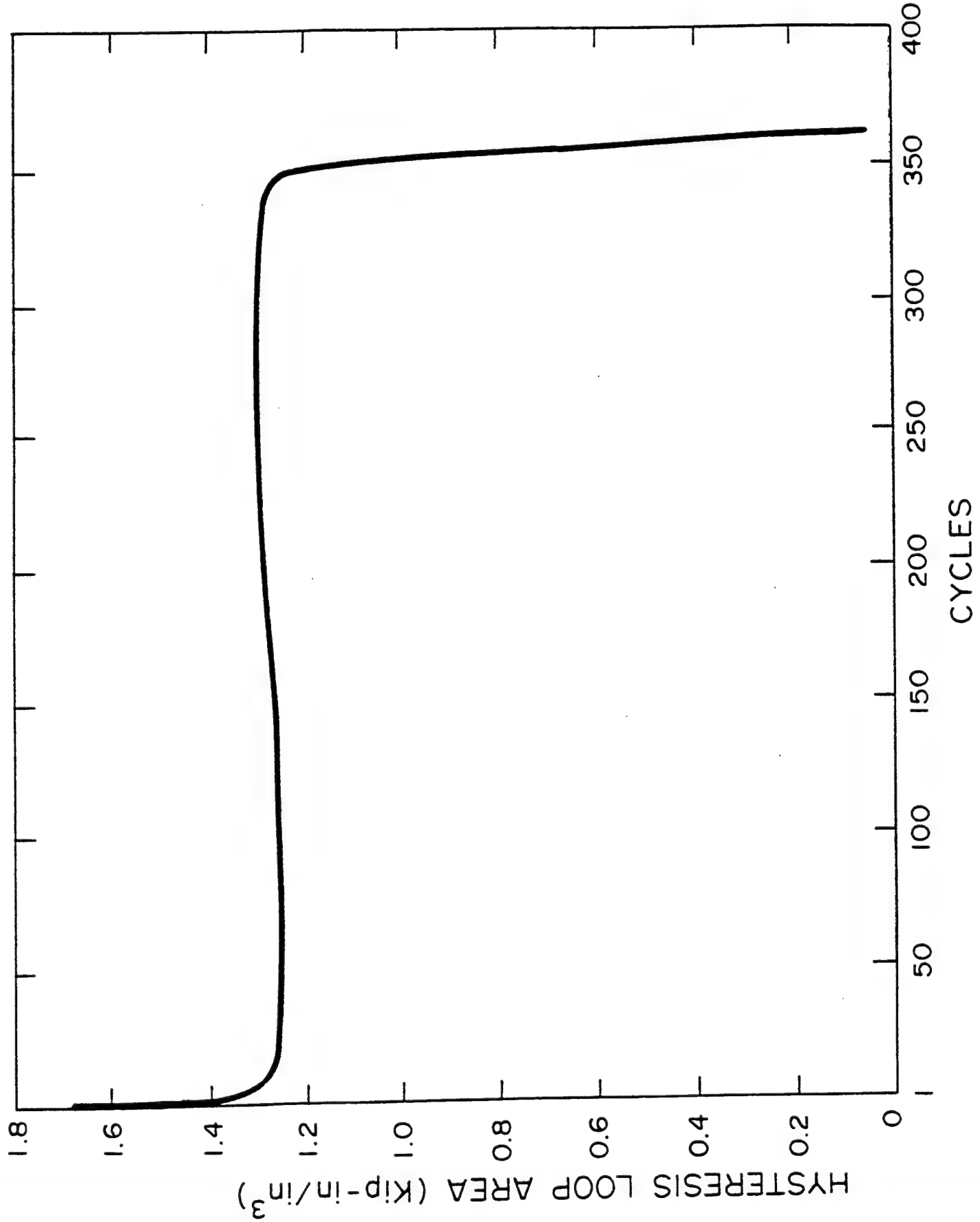
HYSTERESIS LOOP AREA (Kip-in/in^3)
1.8
1.6
1.4
1.2
1.0
0.8
0.6
0.4
0.2
0
1
50
100
150
200
250
300
350
400
CYCLES

Fig. 7

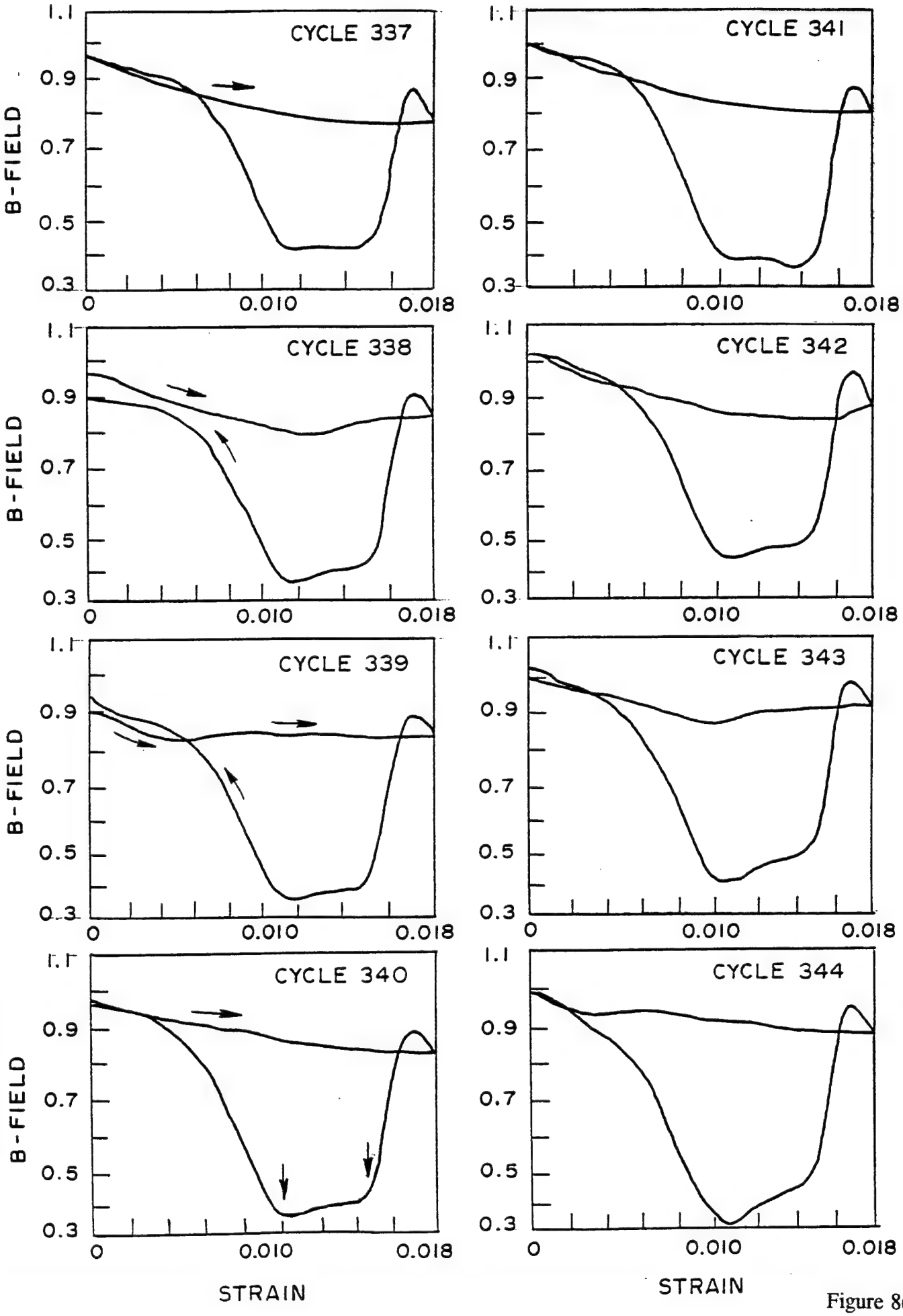
CYCLE 337
CYCLE 341
CYCLE 338
CYCLE 342
CYCLE 339
CYCLE 343
CYCLE 340
CYCLE 344
B-FIELD
STRAIN
1.1
0.9
0.7
0.5
0.3
0
0.010
0.018

Figure 8(a)

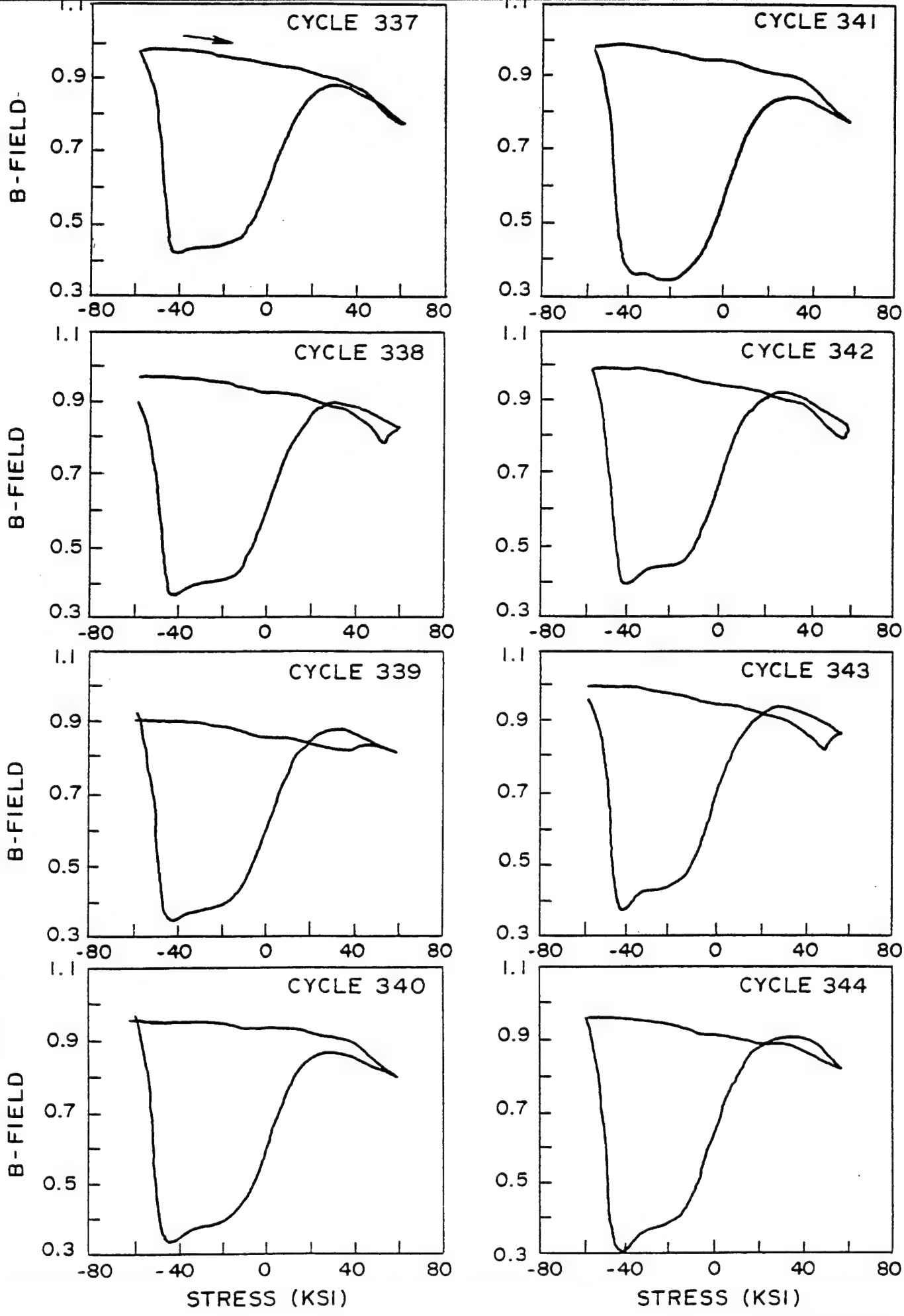
CYCLE 337
CYCLE 341
CYCLE 338
CYCLE 342
CYCLE 339
CYCLE 343
CYCLE 340
CYCLE 344
B-FIELD
1.1
0.9
0.7
0.5
0.3
-80
-40
0
40
80
STRESS (KSI)

Figure 8(b)

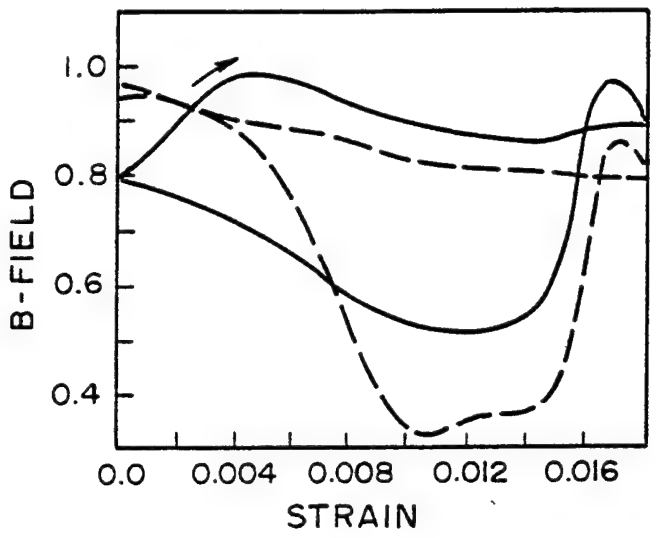
1.0
0.8
0.6
0.4
B-FIELD
0.0
0.004
0.008
0.012
0.016
STRAIN

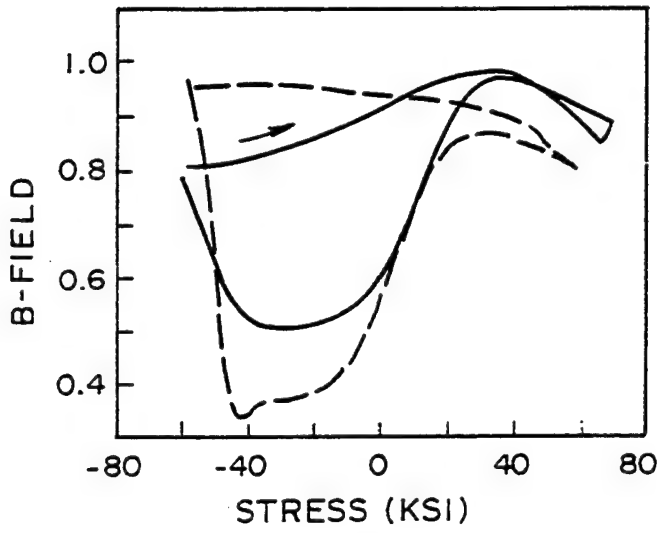
1.0
0.8
0.6
0.4
B-FIELD
-80
-40
0
40
80
STRESS (KSI)

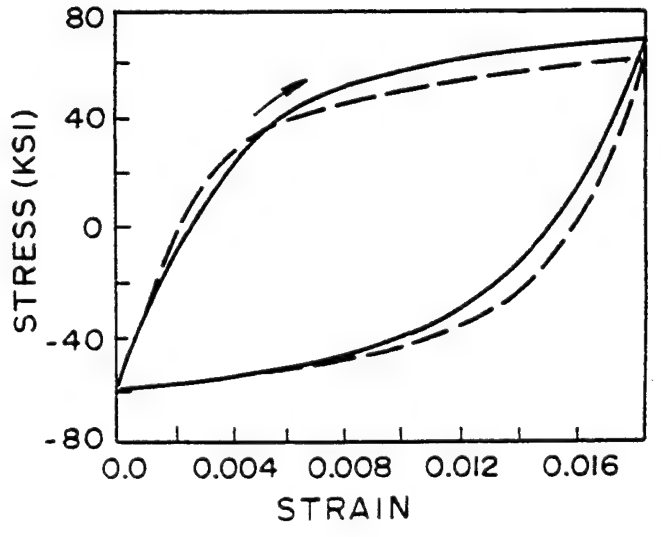
80
40
0
-40
-80
STRESS (KSI)
0.0
0.004
0.008
0.012
0.016
STRAIN

Figure 9

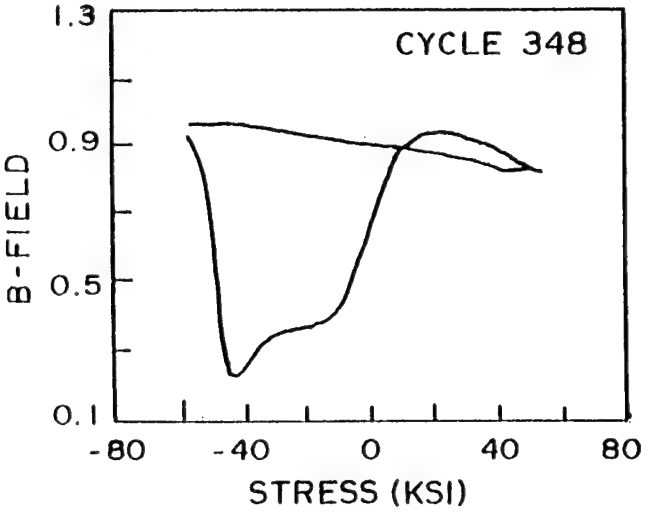
CYCLE 348
B-FIELD
1.3
0.9
0.5
0.1
-80
-40
0
40
80
STRESS (KSI)

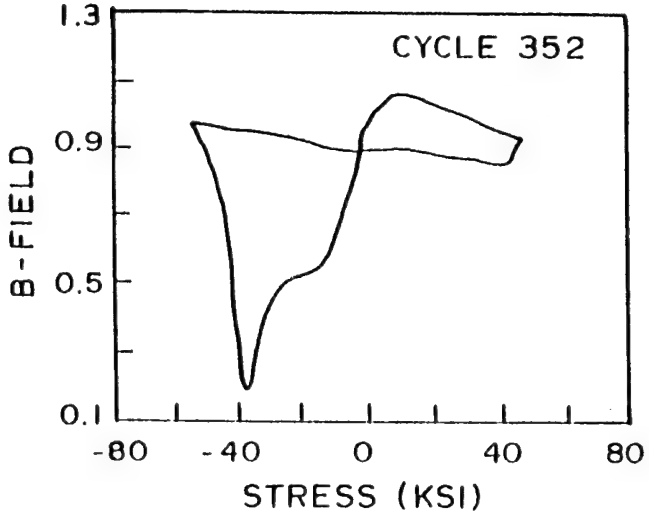
CYCLE 352
B-FIELD
1.3
0.9
0.5
0.1
-80
-40
0
40
80
STRESS (KSI)

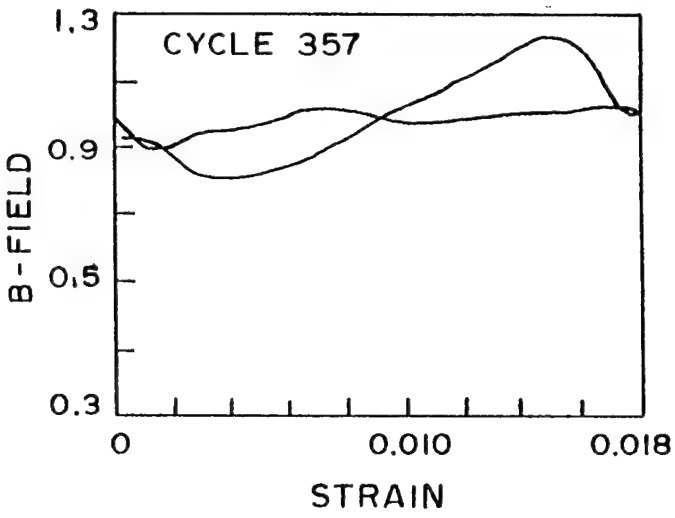
CYCLE 357
B-FIELD
1.3
0.9
0.5
0.3
0
0.010
0.018
STRAIN

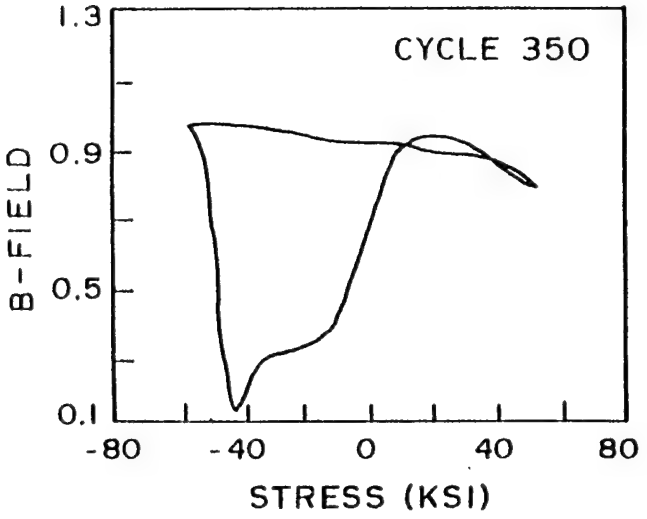
CYCLE 350
B-FIELD
1.3
0.9
0.5
0.1
-80
-40
0
40
80
STRESS (KSI)

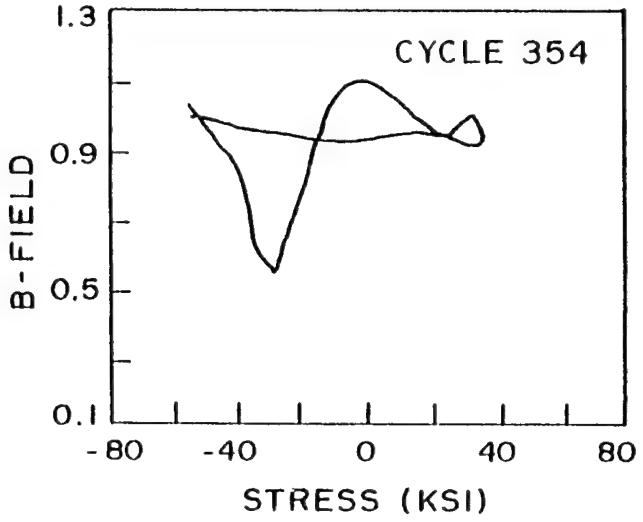
CYCLE 354
B-FIELD
1.3
0.9
0.5
0.1
-80
-40
0
40
80
STRESS (KSI)

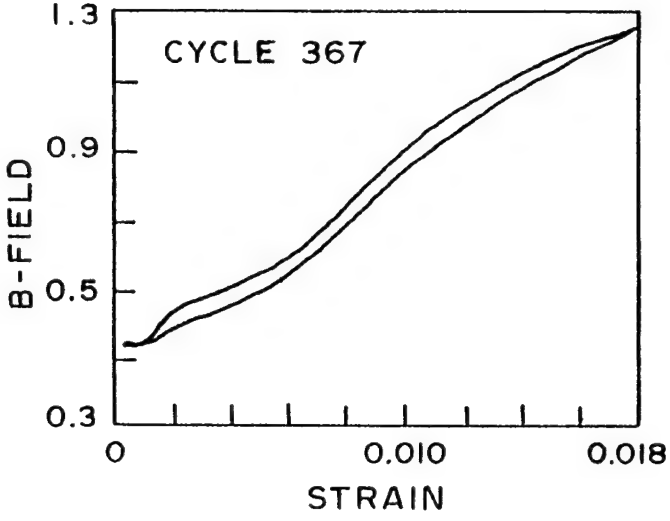
CYCLE 367
B-FIELD
1.3
0.9
0.5
0.3
0
0.010
0.018
STRAIN

Figure 10

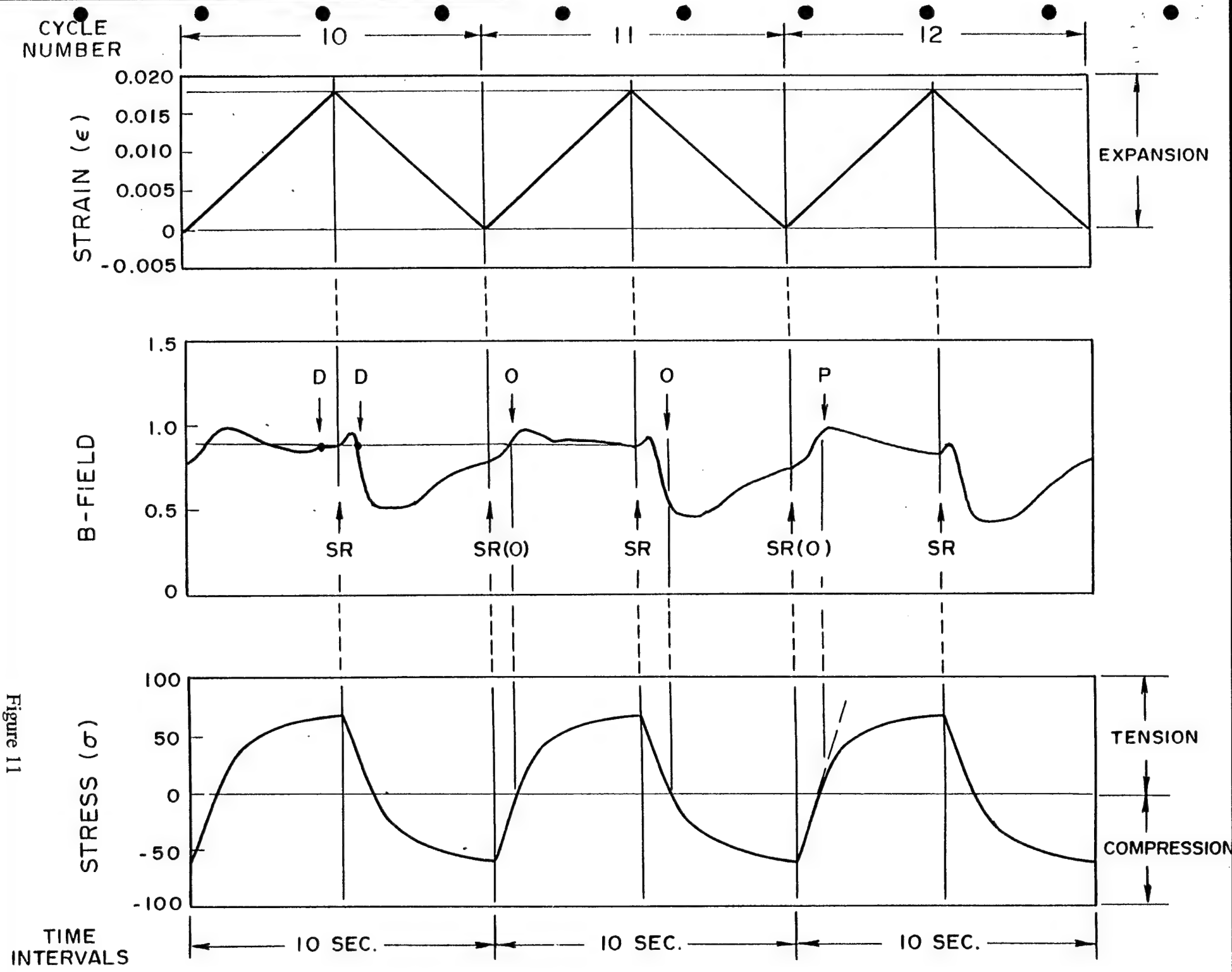
CYCLE NUMBER
10
11
12
STRAIN (ε)
0.020
0.015
0.010
0.005
0
-0.005
EXPANSION
B-FIELD
1.5
1.0
0.5
0
D
D
O
O
P
SR
SR(O)
SR
SR(O)
SR
STRESS (σ)
100
50
0
-50
-100
TENSION
COMPRESSION
TIME INTERVALS
10 SEC.
10 SEC.
10 SEC.

Figure 11

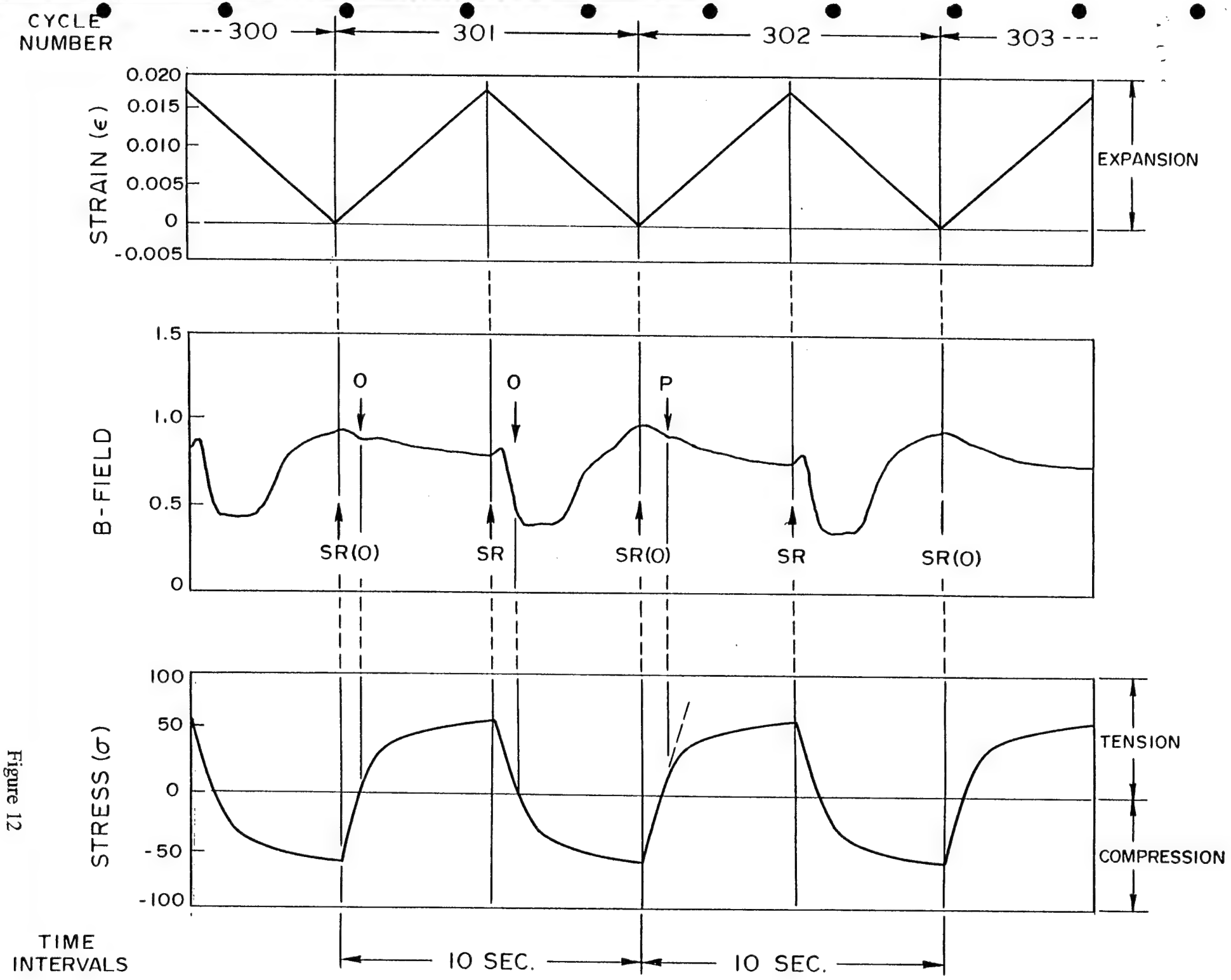
CYCLE NUMBER
---300
301
302
303---
STRAIN (ε)
0.020
0.015
0.010
0.005
0
-0.005
EXPANSION
B-FIELD
1.5
1.0
0.5
0
O
O
P
SR(O)
SR
SR(O)
SR
SR(O)
STRESS (σ)
100
50
0
-50
-100
TENSION
COMPRESSION
TIME INTERVALS
10 SEC.
10 SEC.

Figure 12

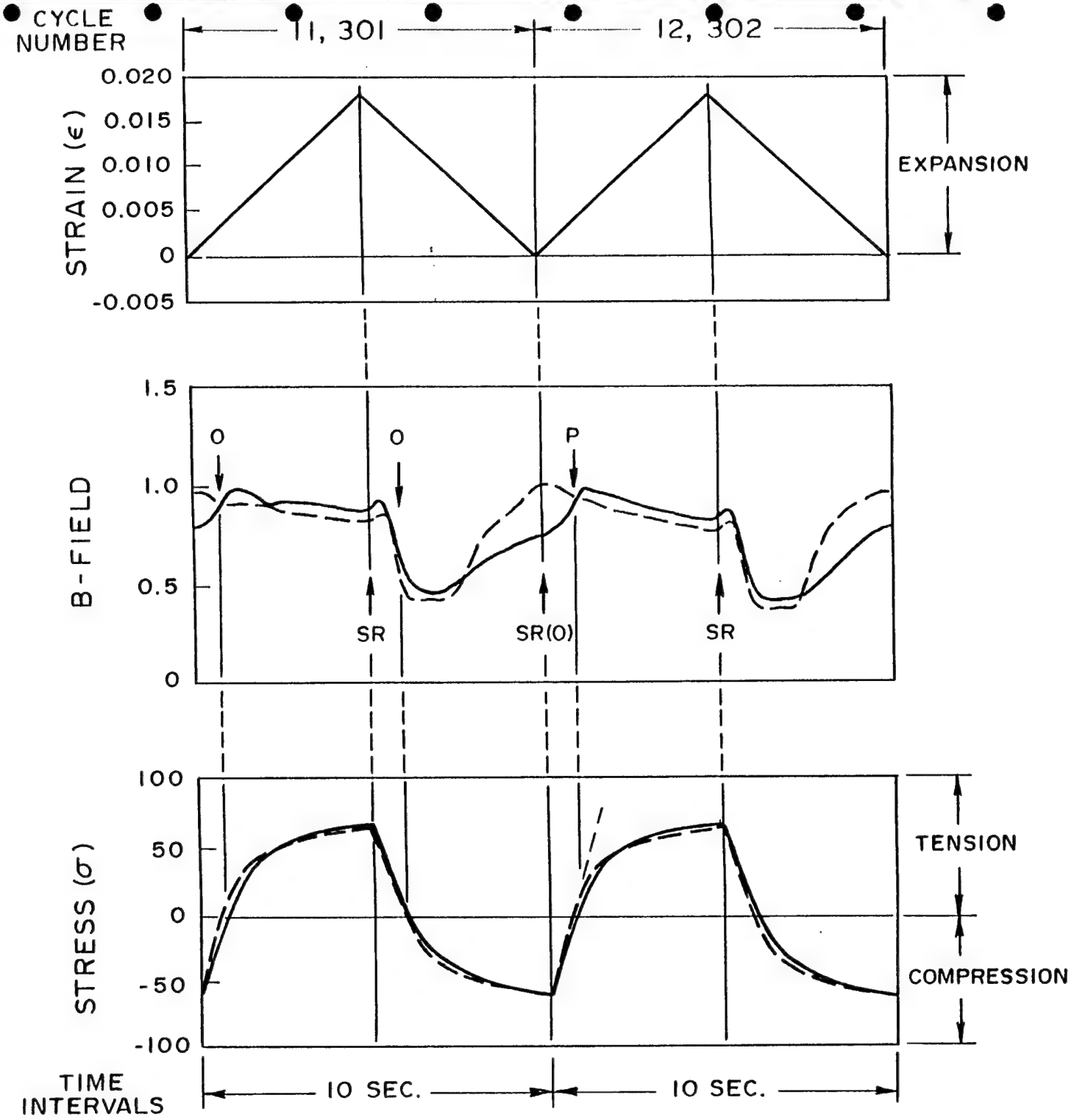
CYCLE NUMBER
11, 301
12, 302
STRAIN (ϵ)
0.020
0.015
0.010
0.005
0
-0.005
EXPANSION
B-FIELD
1.5
1.0
0.5
0
O
O
P
SR
SR(0)
SR
STRESS (σ)
100
50
0
-50
-100
TENSION
COMPRESSION
TIME INTERVALS
10 SEC.
10 SEC.

Fig. 13

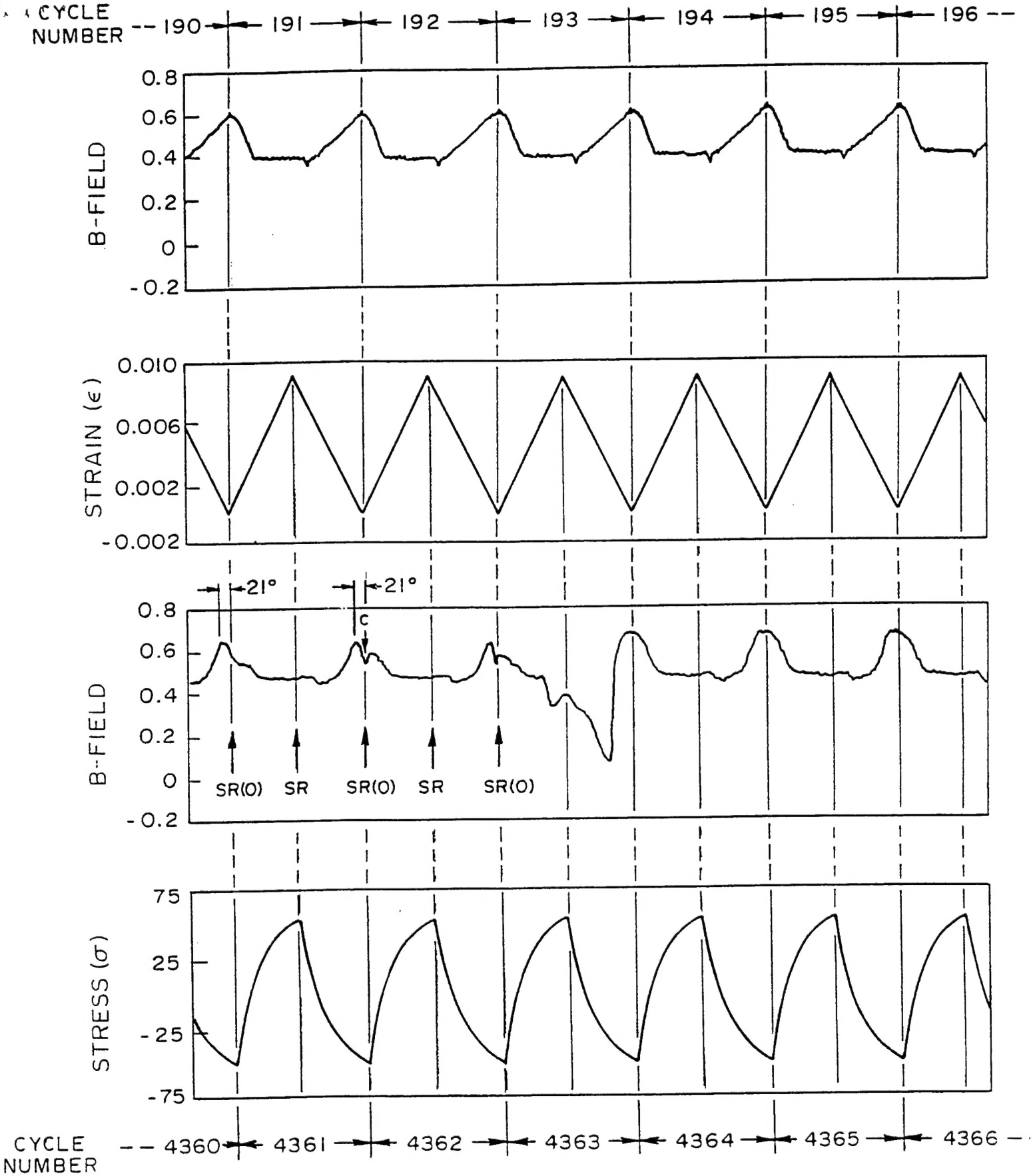
CYCLE NUMBER
-- 190
191
192
193
194
195
196 --
B-FIELD
0.8
0.6
0.4
0.2
0
-0.2
STRAIN (ε)
0.010
0.006
0.002
-0.002
21°
21°
C
SR(0)
SR
SR(0)
SR
SR(0)
STRESS (σ)
75
25
-25
-75
CYCLE NUMBER
-- 4360
4361
4362
4363
4364
4365
4366 --

Fig. 14

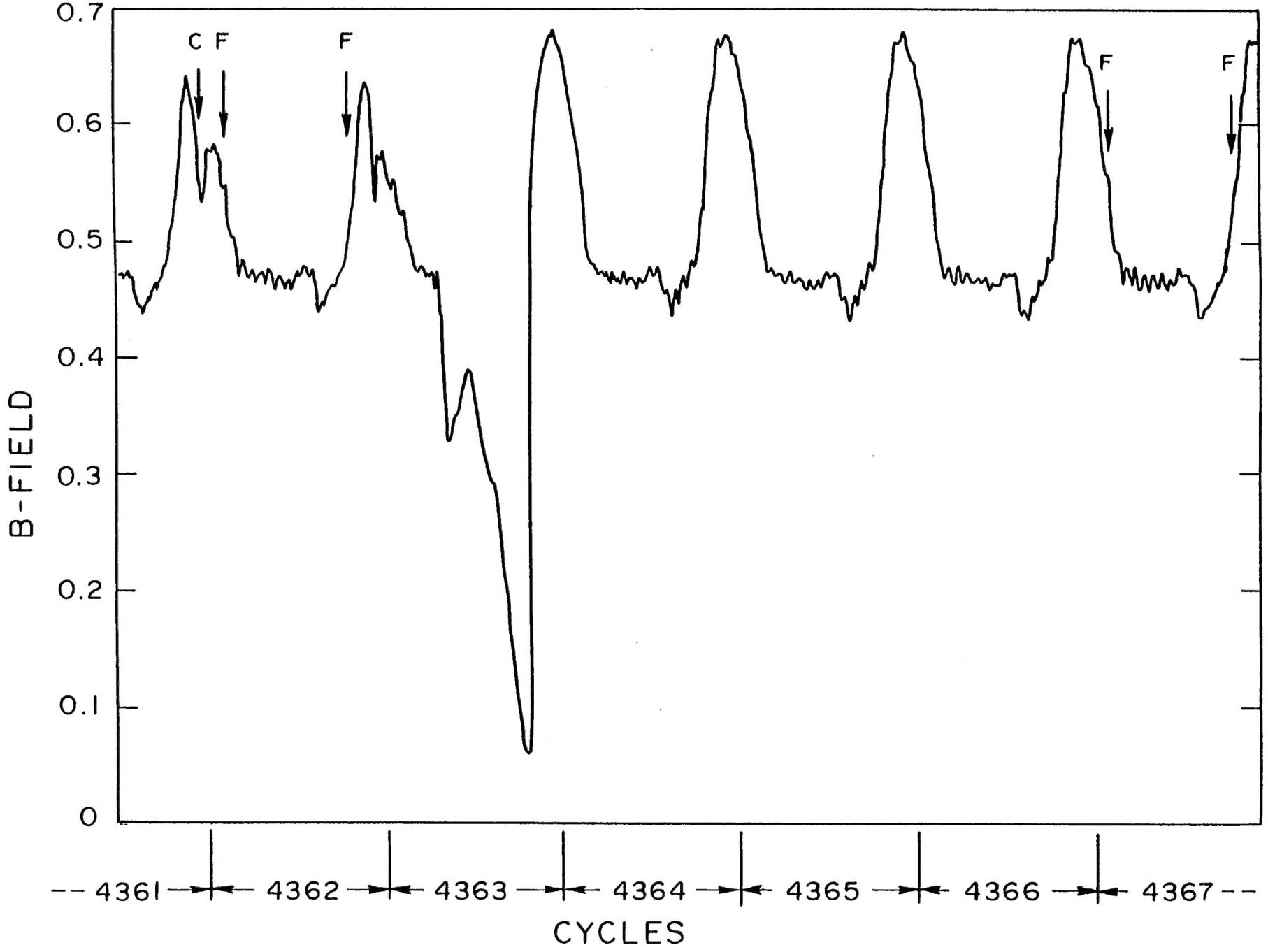
0.7
0.6
0.5
0.4
0.3
0.2
0.1
0
B-FIELD
C F
F
F
F
-- 4361
4362
4363
4364
4365
4366
4367 --
CYCLES

Fig 15

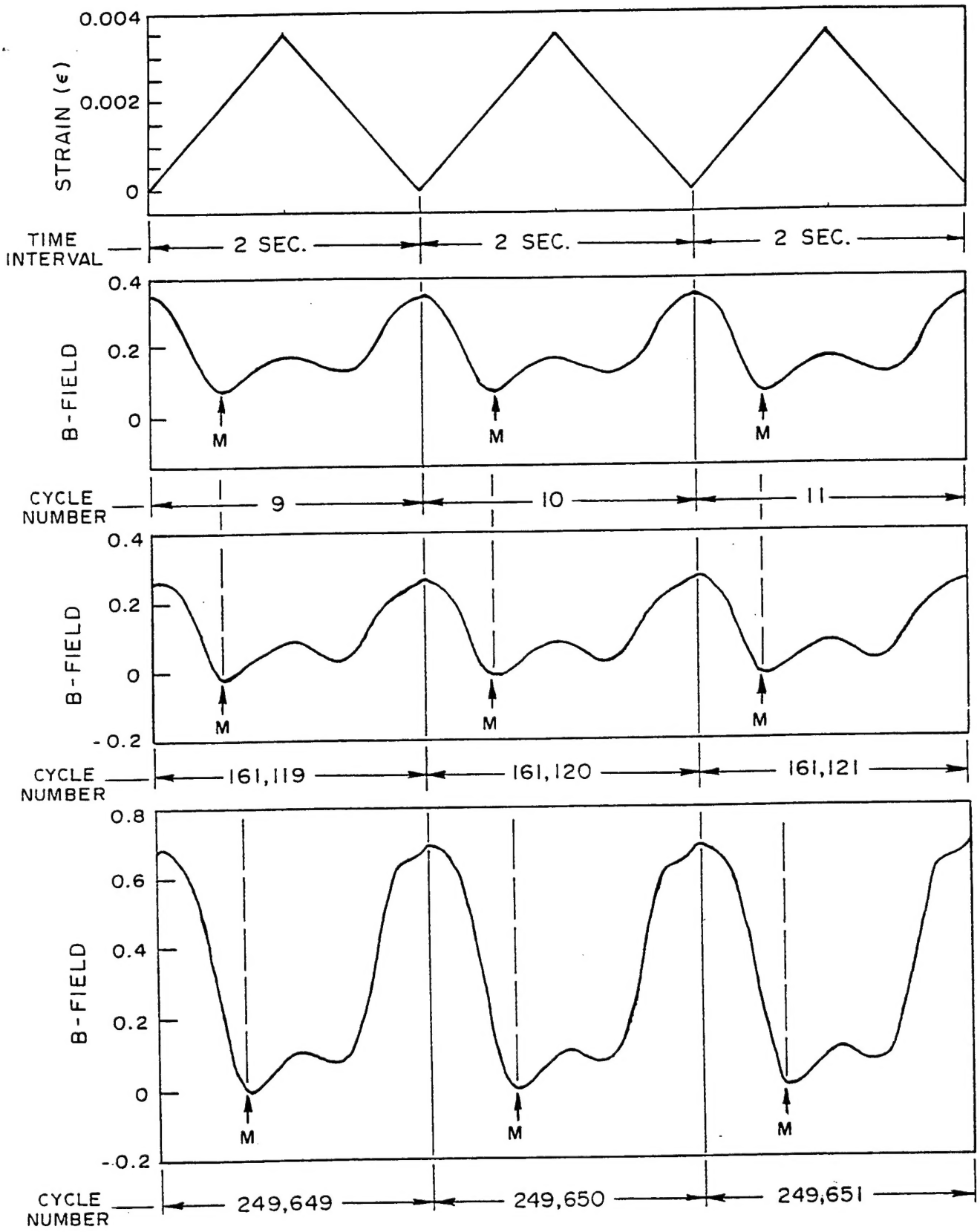
0.004
0.002
0
STRAIN (ϵ)
TIME INTERVAL
2 SEC.
2 SEC.
2 SEC.
0.4
0.2
0
B-FIELD
M
M
M
CYCLE NUMBER
9
10
11
0.4
0.2
0
-0.2
B-FIELD
M
M
M
CYCLE NUMBER
161,119
161,120
161,121
0.8
0.6
0.4
0.2
0
-0.2
B-FIELD
M
M
M
CYCLE NUMBER
249,649
249,650
249,651

Fig. 16

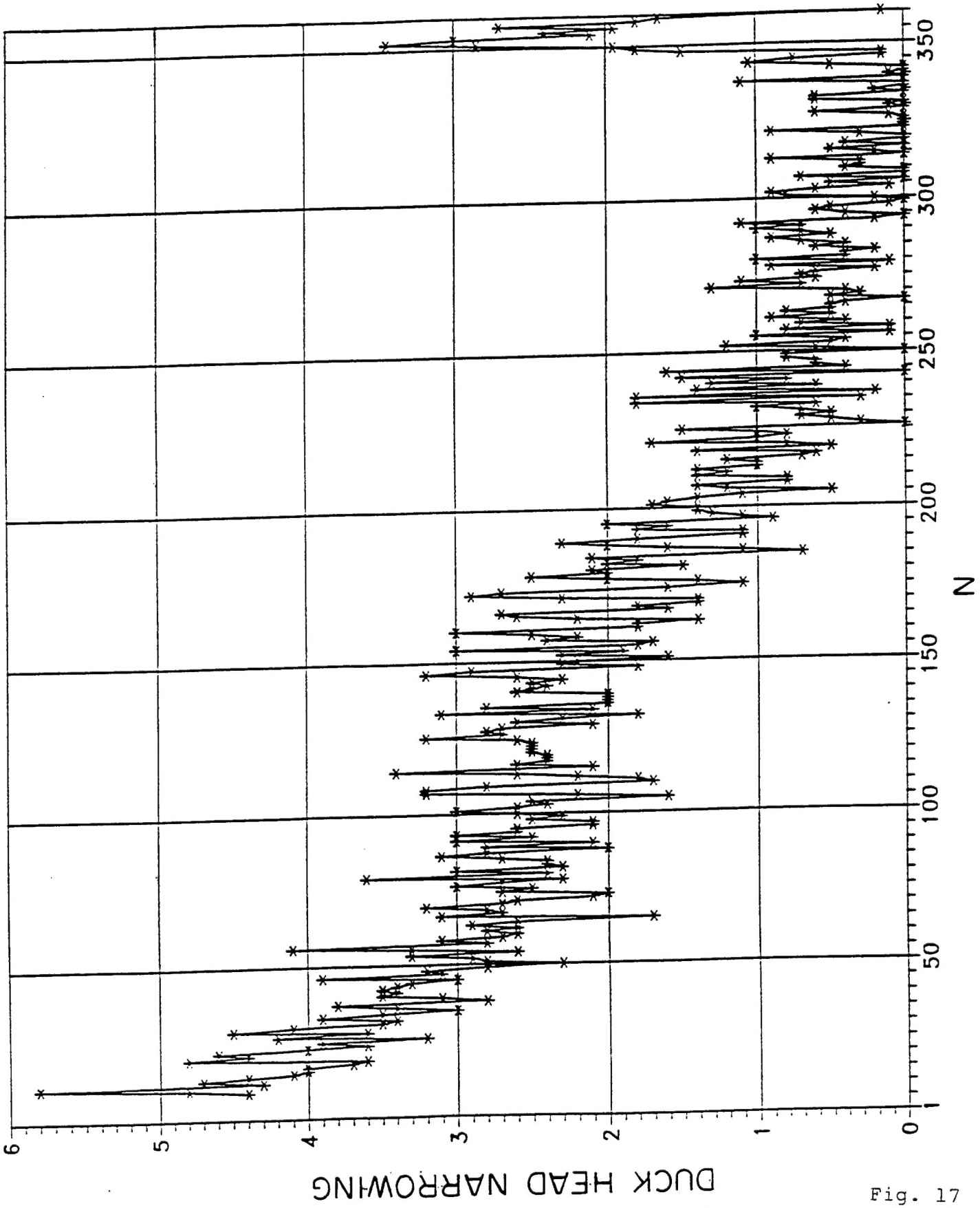

Fig. 17